Advanced Optical A/D Converter

M.C. Hamilton, J.A. Bell, D.A. Leep, J.P. Lin

The Boeing Company
Boeing Defense and Space Group
P.O. Box 3999
Seattle, Washington 98124

1 May 1993

Final Technical Report
Contract N00014-88-C-0285
ARPA Order No. 9537, 87Nov06

ONR

Reporting Period: 29 April 1988 – 30 November 1992

The views and conclusions contained in this document are those of the authors and should not be interpreted as necessarily representing the official policies, either expressed or implied, of the Advanced Research Projects Agency or the U.S. Government.

TABLE OF CONTENTS

LIST OF FIGURES

1.0 INTRODUCTION AND SUMMARY

This program was sponsored by the Defense Advanced Research Projects Agency and the Office of Naval Research to demonstrate the potential of optical techniques for superior wideband analog-to-digital (A/D) conversion. The key performance goals were a signal bandwidth of at least 1.5 GHz with precision of more than 4 bits. The approach should have potential for eventual significant extension beyond these performance levels. Signal bandwidths of more than 10 GHz, with precision of 8 bits, were long term goals.

To summarize the final results, an experimental simulation of a four-channel optical analog-to-digital converter (ADC) operating at 4 GS/s with 2-GHz bandwidth was conducted. The precision obtained in the bandpass sampling mode (near 10 GHz) was 3.8 bits. For baseband signals of up to 2 GHz, the measured precision was 4.6 bits. This performance exceeded the original program goals and constitutes the best known performance obtained with an optics-based ADC approach. The optical ADC technique developed offers potential performance of 10 GHz bandwidth, 20 gigasamples/sec (GS/s) sampling rate, and precision of 6 bits or more. A secondary result from the testing was the development of a data reduction methodology that revealed a previously unreported correlation between jitter and pulse-energy fluctuations. The calculated jitter was twice as small as that derived using a commonly used power spectral density analysis that assumes no correlation between these quantities. This new technique for determining jitter should be of value in future research in high-performance optical ADCs. Several publications have resulted from the work done under this contract (refs. 1-1,2,3).

Advanced military systems transmit, record, and process signals digitally because of advantages in signal-to-noise ratio (SNR), accuracy, and algorithm versatility. Typical system applications include electronic warfare (EW) receivers, signal intercept, radar processing, and digital transmission links. As most raw data are collected in analog form, ADCs are needed to make the transition from the analog to the digital domain. These systems have entered the multigigahertz-bandwidth regime, with carrier frequencies in the microwave and the millimeter-wave range. Ever faster ADCs are required as their bandwidths continue to increase.

Current electronic ADCs digitize signals at frequencies of only a little more than 1 GHz, with precision of less than 5 bits at their full bandwidth. This limitation is due to instabilities in their complex, high-speed circuits and cross-coupling between signals, clocks, and data. To realize the maximum advantage from using digital techniques in emerging wideband systems, ADCs are needed with signal bandwidths greatly exceeding 1 GHz and corresponding sample rates. They should provide as much precision as possible, although precision of as few as 2 bits can be of value in some applications (e.g., where gain results from a signal processing algorithm). Reduced precision is tolerable also in applications where automatic gain control is allowed.

The approach initially chosen was based on a concept invented by H. F. Taylor (ref. 1-4) and first demonstrated by R. A. Becker (ref. 1-5), et al. at MIT Lincoln Laboratory. A 4-bit version of the concept is shown in figure 1-1(a). In this approach, the signal to be digitized is simultaneously

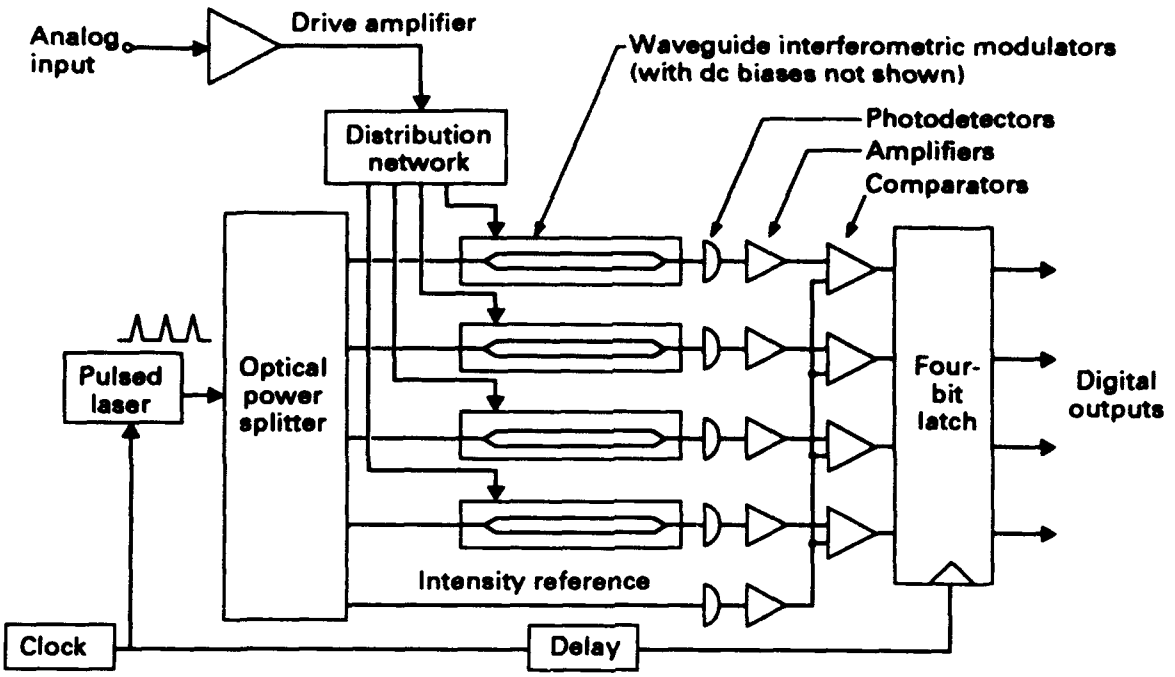

(a) Four-Bit Architecture

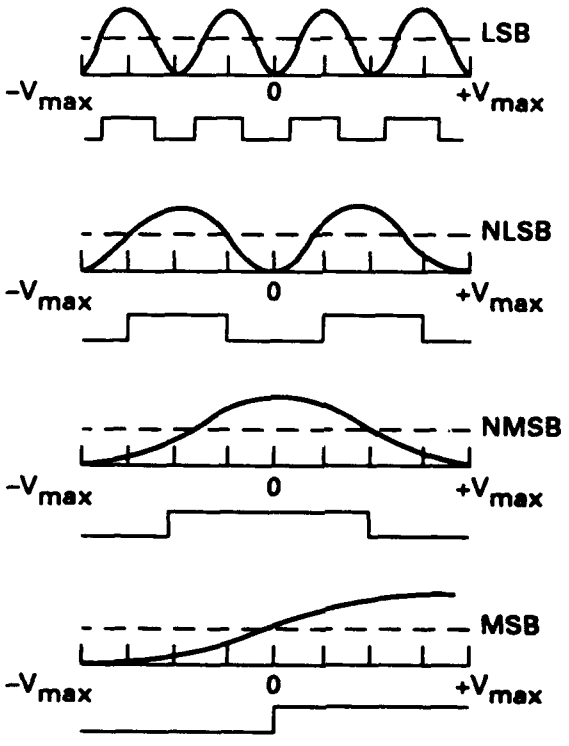

(b) Intensity vs. Voltage

Figure 1-1. Mostly Optical ADC Concept Invented by H. F. Taylor: (a) Schematic for 4-Bit Version. (b) Light Versus Voltage Characteristics for the Modulator Manifold

applied to a set of optical waveguide intensity modulators whose voltage responses differ by successive factors of 2. These responses can be realized in one of two ways. The first is by an equal power split of the signal among modulators whose electrodes differ in length by factors of 2. The second is by unequal power splitting among identical modulators such that the applied voltages differ by factors of 2. In either case, the resulting voltage responses are as shown in figure 1-1(b). The most sensitive modulation channel corresponds to the least-significant-bit (LSB) of the ADC and so on through the least sensitive channel. The signal voltage applied to the modulator manifold is sampled by a train of ultrashort light pulses of equal intensity. The light output of each modulator is detected and electronically compared with a reference intensity to determine whether it is above or below a threshold level. Examination of the set of response characteristics shows that every quantized input voltage level has a unique set of output states for the four modulators. The set of latched outputs of the comparators constitute a 4-bit word representing the input-signal voltage level.

A prototype of the type described above was the most advanced optical ADC yet demonstrated at the beginning of this program. Reference 1-2 reported 2-bit precision at 1 GS/s. The sampling rate was limited by the speed of then-available electronic comparators. The modulators used had unequal-length, lumped-element electrodes that limited the bandwidth to about 1 GHz or so.

The strategy planned initially in this contract program was to extend the performance of the Taylor approach by making improvements in several areas. The first was to employ the unequal power distribution scheme for coupling the signal into the modulator manifold. The advantage to that is because all of the electrodes are identical, the frequency responses of all the modulators are the same. A second planned improvement was a traveling-wave electrode design to extend the ADC bandwidth. A novel electrode structure that would improve the velocity-match between signal and optical waves was also planned. Finally, faster electronic comparators (commercially obtained) were to be used to allow an increased sampling rate.

The Taylor approach imposes stringent requirements in two areas that limit its potential.

a. The LSB modulator must be driven through many cycles. Even with velocity-matched traveling-wave electrodes for improving the efficiency, relatively high input power levels would be required to achieve a precision of even 4 bits. This situation is aggravated by the required power splitting among the electrodes.

b. Because one cycle of signal oscillation produces many cycles of oscillation in the output of the LSB modulator, the comparator operation is particularly sensitive to jitter in the optical- pulse train.

A final limitation of the approach applies to the sampling rate. Even though mode-locked lasers with very high pulse rates were known, the sampling rate is limited by the speed of electronic comparators, just as for electronic ADCs.

Early on in the program, an alternative approach that offers higher potential performance became known that does not suffer from the limitations of the Taylor ADC approach. In the new approach, the signal is also sampled by an optical pulse train. However, the signal drives a single modulator in the small signal regime resulting in an envelope modulation of the output pulse train. This high speed data stream is time demultiplexed into parallel data channels in which electronic digitization is performed on the detected optical pulses. Thus, this architecture is actually a hybrid in which the best capabilities of optics and electronics are combined. In the remainder of this report, we refer to it as the hybrid optical/electronic A/D converter (HOE-ADC). Optics is used for high-speed sampling, wideband modulation, and high-speed demultiplexing. Electronics is used for high-precision digitizing and data storage. This approach is described in more detail in section 2.1.

A prototype of the HOE-ADC was implemented and tested under a Boeing IR&D program. This four-channel version operated at 2 GS/s and attained a little over 2 bits precision. Several factors combined to limit the performance.

a. The gain-switched laser had jitter well exceeding 1 ps.
b. The optical path had a net loss approaching 20 dB, which degraded the SNR.
c. The multichannel electronic digitizers (commercially obtained) compromised performance because of internal timing errors. Despite these factors, the measured performance was the most advanced known at that time.

Considering the previously discussed limitations of the Taylor approach and the promising potential of the HOE-ADC, the sponsor concurred with adopting the new approach for the remainder of the program. Several improvements were planned over the prototype first tested in the IR&D program. First, and probably most important, was to incorporate an actively mode-locked laser in place of the gain-switched laser. The two-fold benefits expected were to reduce jitter to below 1 ps and to allow higher sampling rates. The laser wavelength was changed from 1,300 nm to 1,530 nm to allow use of a fiber-optic amplifier for increasing the SNR. Finally, a new switch array incorporating a novel "digital" switch design was to be developed. This type of switch is more robust in maintaining low crosstalk without precise setting of the drive voltages.

The execution and findings of the program are described in some detail in the following sections. In section 2.0 we discuss the operating principle of the HOE-ADC and the characteristics of the key components used in our implementation. This section also addresses limitations in performance due to various noise sources. Finally, section 2.0 presents test results for the first prototype that operated at 2 GS/s. Section 3.0 describes the effort aimed at development an advanced 1x4 switch array for the second prototype HOE-ADC. Section 4.0 describes the configuration of the second prototype HOE-ADC and the results from testing it in a single-channel experimental simulation at 4 GS/s.

2.0 APPROACH

2.1 HOE-ADC Architecture

The basic idea for the HOE-ADC is to combine the high bandwidth of electro-optical sampling with the precision of electronic A/D converters. By demultiplexing the optical samples, it becomes possible to use multiple electronic A/D converters that operate in parallel with each being clocked at a slower rate than the overall system sampling rate.

The HOE-ADC approach uses time-demultiplexing of the optical samples as shown in figure 2-1. Similar to the approach of reference 1-1, the electro-optical sampling takes place within an integrated intensity modulator. The optical input to the modulator comes from a pulsed laser operating at a frequency, F_S, and the energy of the transmitted pulses would ideally be linearly related to the input signal voltage applied during the corresponding sampling time. The resulting intensity-modulated optical pulse train is time-demultiplexed into M channels using a tree array of M-1 electrically controlled optical switches. The switches and laser are driven synchronously so that each pulse is directed to a single output channel at a rate reduced from the input by M^{-1}. Each output channel of the demultiplexer is followed by a photodetector, amplifier and electronic A/D converter that samples the peak amplitude of each pulse at a frequency of F_S/M. Our first laboratory demonstration of this approach had M=4, (as shown in fig. 2-1), and the laser pulse rate was 2 GHz. This system overcomes the problems mentioned earlier for the approach of ref. 1-1. By operating multiple A/D converters in parallel, the optical sampling can proceed at a rate faster than the electronic A/D converters are capable of individually. Similar time deinterleaved techniques have been successfully applied to increase the sampling rate of all-electronic A/D converters (refs. 2-1, 2-2). Also, the input drive power is much reduced in this approach since only one electro-optical modulator is used for the sampling, and the full scale range of the drive voltage is restricted to a portion of the transfer function that is approximately linear.

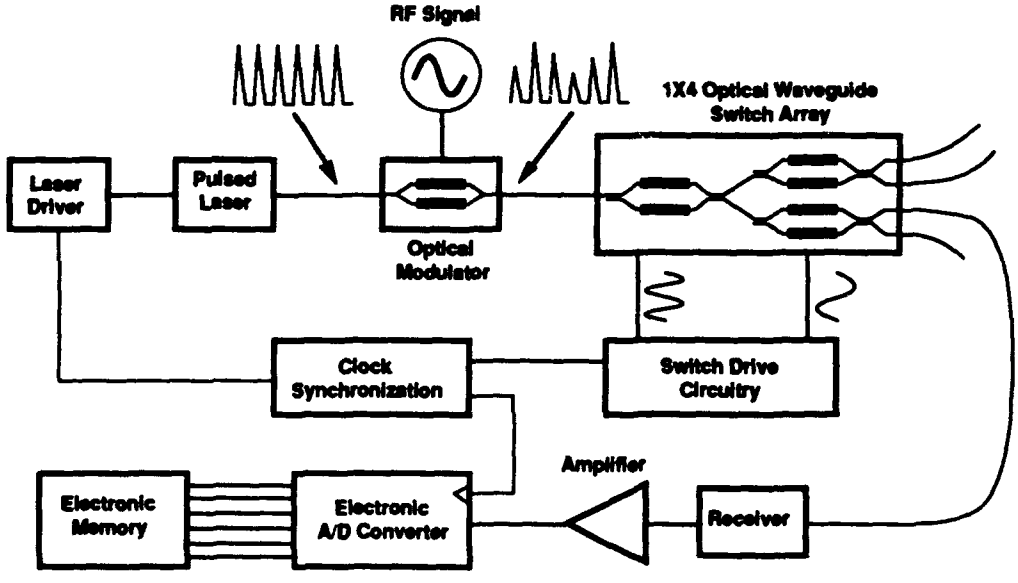

Figure 2-1. Block Diagram of a Four-Channel Hybrid Optical/Electronic A/D Converter

Some signal processing applications make use of only a small relative bandwidth and are especially sensitive to the fidelity of the signal phase. One approach to sample such signals is to heterodyne the signal with a local oscillator and perform the sampling at baseband. An alternative approach, which avoids the phase aberrations that can be introduced by electronic mixers, is to sample the narrowband signal directly. The frequency domain picture of this situation is in figure 2-2. In this approach, the signal bandwidth must be limited to not exceed the Nyquist bandwidth (which is half of the sampling frequency), and the sampling aperture time must be small compared to a period of the highest signal frequency. The HOE-ADC demonstration system discussed in this report adopts this approach to sample a signal in the 10- to 11-GHz band using a sample rate of 2 GS/s.

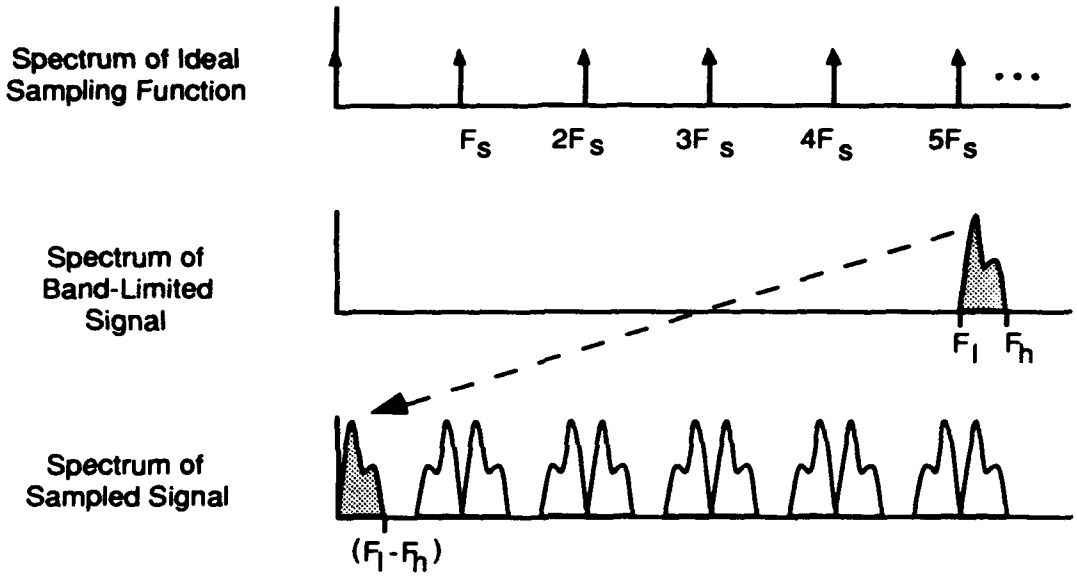

Figure 2-2. Bandpass Sampling Concept

2.2 HOE-ADC Components

The HOE-ADC architecture combines several optical and electronic components each of which must meet some minimum requirements in order to yield a high-fidelity system. The general properties of these components, together with some properties specific to our demonstration system, are now discussed in their order along the path from the laser to the receiver. In this section, where specific component properties are mentioned, they apply to the four-channel test system. Test results from this system are the topic of section 2.4. The most recent one-channel tests conducted under the contract made several component substitutions from this four-channel system. These are described in section 4.0.

2.2.1 Pulsed Laser

The requirements of the pulsed laser are certainly the most demanding of any single component in the HOE-ADC system. Since the pulse frequency corresponds to the HOE-ADC sample rate,

favorable competition with electronic A/D converters implies that the laser should be extendable to pulse rates of 10 to 20 GHz. As discussed later in this section, the precision of the samples is affected by pulse timing fluctuations and by relative intensity noise (RIN), which leads to fluctuations in the laser pulse energy, E_p. There also should be enough energy in each pulse so that, when accounting for the insertion loss of the optical components, shot noise does not significantly limit the precision. Typically, average powers of at least a few milliwatts and timing jitter below 1 ps are required for the precision to be of interest.

The laser must also produce pulses of short duration in order to obtain high-fidelity A/D conversion. This is due in part to the low-pass filtering effect of sampling an analog signal with a non-zero aperture duration (or time-averaging period). The effect this has on the frequency response of the system can be determined by examining the Fourier transform of a single sampling pulse. For example, taking the pulsewidth to be 35 ps and of Gaussian shape, (representative of the gain-switched diode lasers discussed later), a rolloff of 0.8 dB is expected across the 10- to 11-GHz band. Subpicosecond pulsewidths have been demonstrated using mode-locked diode lasers (refs. 2-3, 2-4 and 2-5), and thus, the contribution to nonlevel frequency response attributed to this effect is potentially negligible compared with other band-limiting components, namely, the modulator and related drive electronics. In the case of conventional baseband sampling, it is important to note that pulses with duty cycles of 20% of the pulse period may be quite acceptable. It is likely that more than one of the pulsed sources considered here would be acceptable for a given application based on technical requirements. The deciding factors would then become cost and reliability, neither of which are considered here.

Several instruments are typically required to determine the characteristics of a pulsed laser for the HOE-ADC: (1) optical power meter, (2) optical spectrum analyzer, (3) high-speed photodetector, (4) high-speed sampling oscilloscope, and (5) microwave-spectrum analyzer. The laser characteristics depend on the operating conditions; thus in practice one characterizes a pulsed-laser "system" that includes a bias-current supply, temperature stabilizer, RF drive circuit, optomechanical components, and, perhaps, an optical isolator. The primary use of the sampling oscilloscope is to measure the pulse width and shape. This time-domain view also allows the light level between pulses to be measured. The presence of such background light could significantly corrupt the electro-optical sampling process.

To measure the stability of the pulsed sources, a microwave spectrum analyzer is used together with a wideband photodetector. We found significant disagreement among researchers in this field concerning the relationship between spectral noise-power density and pulse jitter. Through an analytical treatment, numerical modeling, and comparison with our measured spectra, we have resolved this issue (ref. 1-5). By integrating the noise power over frequencies between harmonics of the pulse rate and by observing how the noise depends on the order of the harmonic, it is possible to separately determine the jitter and intensity fluctuations of the pulses.

We have used diode lasers to generate optical pulses by two separate methods: gain-switching and active mode-locking. In the case of mode-locking, the period of the electrical drive signal (or a

multiple of the period) is matched to the round-trip time for light in the laser cavity. Thus, within a narrow-frequency range, the pulse rate of the laser is determined by its cavity length. Gain switching also involves driving the laser with a periodic current, either pulsed or sinusoidal, and has the advantages of being nonresonant and easily packaged. However, with this type of drive, each pulse from the laser must originate from spontaneous emission and is inherently less stable than a mode-locked laser in which the gain medium is stimulated by recirculating pulses in the laser cavity. The appeal of a mode-locked diode laser for the HOE-ADC is based on demonstrated high pulse rates (16 GHz in the case of ref. 2-6) and high stability (phase noise measurements of the pulsed light suggest that the timing jitter is limited primarily by the drive electronics to between 0.3 and 1 ps).

The diode laser used in our four-channel system demonstration was an Ortel model 1510B Fabry-Perot cavity that was gain switched by driving it from a 2-GHz pulsed electrical source. This laser operates at a wavelength of 1,300 nm, and delivers 290 μW of average power from the tip of its single-mode fiber pigtail. The electrical impulses were produced by a step recovery diode, Hewlett-Packard model 33005CH20, driven by a 27-dBm sine wave. Although the electrical pulses going to the laser were roughly 50-ps wide, the pulses emitted from the laser were measured with a fast photodiode, Tektronix SD-46, together with a Tektronix 11802 sampling oscilloscope to have a pulse width (full width at half-maximum) of 33 ps. Measurements of this laser with the microwave spectrum analyzer showed that the noise was primarily due to a pulse-timing jitter of 1.7 ps. Separate spectral measurements of the electrical pulse train showed that the timing jitter of the drive was about 0.1 ps, and was negligable compared with the jitter of the laser pulses. We also looked at 4-GHz pulses from this laser, produced by direct sine wave driving, and found the jitter to be 1.2 ps. Although this gain-switched-diode laser is far simpler to obtain than a mode-locked laser of similar power and pulse rate, the results discussed later in this report show that the associated jitter is a significant source of error.

Based on the performance analysis derived in section 2.3, the power we expected to obtain from a pulsed semiconductor laser, and the anticipated losses of the waveguide components, we concluded that optical amplification would be required for the HOE-ADC system precision to reach the 5- to 6-bit range. With this in mind, the next pulsed laser source we obtained had a wavelength of 1,530 nm to be compatible with an erbium-doped fiber amplifier (EDFA) that we purchased (BT&D model EFA-3000). This laser, Lasertron model QLM5S990, has a distributed feedback cavity and was packaged with a fiber pigtail. We initially operated this laser in the same gain-switched mode as described above for the Ortel laser. By again characterizing the spectral noise, we found the Lasertron laser to have substantially more jitter than the Ortel model under both the 2- and the 4-GHz drive conditions: 6.5 and 4.2 ps respectively. Following these tests, we modified the fiber pigtail of the Lasertron device by cutting it to a short stub so that the roundtrip extended-cavity resonance was roughly 2 GHz. We deposited a coating on the fiber with a reflectivity of roughly 50% so that a significant portion of each pulse would return to seed subsequent pulses and effectively modelock the laser. Although our primary interest was in operating the laser at a pulse rate of 4 GHz, we decided against this choice of a cavity-resonance frequency because the fiber stub could not be practically prepared. With the 2-GHz cavity resonance, we were able to obtain improved pulse stability at both the 2- and the 4-GHz drive conditions compared with the measurements performed before the cavity modification. From spectral noise measurements, the jitter for a 2-GHz pulse rate was decreased to

1.4 ps and the jitter at 4 GHz was 0.6 ps. The mean optical power from this modified laser was only 45 μw, but, following the EDFA, the power was boosted 17 dB to 2.4 mW. This measurement accounts for the losses from two optical isolators placed before and after the EDFA and a tunable bandpass filter (JDS Fitel model TB-1570) that blocks most of the broadband amplified spontaneous emission. This pulsed-laser system was used to carry out the single-channel demonstration that was the concluding activity within the scope of the contract.

2.2.2 Intensity Modulator

The electro-optical sampling employed by the HOE-ADC depends on a modulator that transforms an input voltage to an optical transmission. In this section we discuss a conventional interferometric modulator of the type used in the HOE-ADC system demonstrations. A more elaborate modulator that offers an improved linearity is the subject of the next section.

Electro-optical intensity modulators are typically based on interferometers in which the phase difference between the separate optical paths varies linearly with applied voltage. A complication is that the transmission, T, does not vary linearly with the voltage, V, but rather has the form:

$$T = \frac{T_0}{2}\left[1 + \sin\left(\frac{\pi V}{V_\pi} + \phi\right)\right] \tag{2-1}$$

where V_π is the switching voltage and ϕ is an offset that is typically controlled with a bias voltage. To obtain a nearly linear response, ϕ is adjusted to be some multiple of π so that the transmission is midscale.

It is apparent from the standpoint of noise, resulting from limited laser power or intensity fluctuations, that a full-scale input signal should drive the modulator over as large a transmission range as possible. However, the nonlinear response of the modulator imposes a limitation on the allowable modulation depth, m, which we define as:

$$m = \frac{T_{max} - T_{min}}{T_{max} + T_{min}} \tag{2-2}$$

where T_{max} and T_{min} are the maximum and the minimum transmissions over the full-scale range of the signal input voltage. If m is too large, the sampled signal becomes significantly distorted by the harmonics and intermodulation products between separate signal frequencies. The most direct approach toward obtaining a larger acceptable modulation index is to change the modulator characteristics to improve linearity; (this is the next subject within this section). Difficulties associated with linearizing the modulator response must be weighed against the indirect approach of compensating for the nonlinearity. This could be accomplished either by modifying the transfer characteristics of an analog component following each detector or by applying a digital lookup table following the electronic A/D converters.

We have employed a variety of methods to measure the sensitivity (or equivalently, the switching voltage—V_π), of Mach-Zehnder intensity modulators. The method we have found to be most useful

can be easily accomplished at any drive frequency using a detector that responds only to the average transmitted power. Making use of the known nonlinear response given by equation 2-1, the *minimum* time-averaged transmitted optical power, $\overline{P}$, is related analytically to the switching voltage and the amplitude, V, of a sinusoidal drive voltage according to:

$$\overline{P} = \frac{P_{max}}{2}\left[1 - J_0\left(\frac{\pi V}{V_\pi}\right)\right] \tag{2-3}$$

where J_0 is the Bessel function of the first kind and P_{max} is the maximum transmitted power when the applied voltage is constant. This equation can be solved iteratively for V_π. Measurements of the power maximum, P_{max}, and the minimum $\overline{P}$, depend on varying the modulator bias point. A measurement of V is typically based on an RF power meter. The advantages of this approach are (1) measurements can be made at any desired drive frequency, (2) no compensation is required for the frequency response of the detector, and (3) good results are obtainable even for low drive amplitudes (though this can depend on making a correction for the minimum transmission without RF drive). This same principle can be applied to measuring the frequency response of a modulator.

The modulator used in our four-channel HOE-ADC system was obtained from Hoechst Celanese (actually fabricated by GEC Marconi) and uses a $LiNbO_3$ integrated Mach-Zehnder interferometer and traveling-wave electrodes for the signal input. The frequency response is level within ± 3 dB from 1 to 18 GHz, and over our 1 GHz band of 10 to 11 GHz, the response varies less than ± 1 dB. The switching voltage for a 50Ω source at 10.5 GHz was determined to be 25V, and is considerably higher than what is expected from a device that is resonantly matched to our 1-GHz signal bandwidth. Polarization-preserving fiber pigtails are attached to the input and output of the modulator to minimize optical losses in the system. The optical insertion loss from fiber to fiber for this modulator, when set to maximum transmission, is 5.2 dB. The bias of the modulator was adjustable using a separate set of input electrodes and did not require any drift correction over the time scale of hours in our lab. However, the optimal bias point of the modulator varied linearly with applied electrical power with a slope of 1.9 rad/W. This bias shift is attributed to a thermal effect because it has a time constant of roughly 1 second. This problem is quite typical for this type of modulator, and could be remedied by including a low-frequency control loop that maintains the average detected power at a level corresponding to the midpoint of the modulation range.

2.2.3 Optical Switch Array

Time demultiplexing of the light pulses transmitted through the modulator is accomplished by using optical switches, each of which has one input and two complementary outputs. The switches are similar in function to the Mach-Zehnder interferometer used for the modulator except that access to both output ports is required. The first switch in the binary tree structure is driven at a frequency of half the sample rate, $F_S/2$, and with the correct phase, amplitude, and bias, so that the light pulses are sent alternately to the two separate outputs. In the case of a four-channel HOE-ADC, one more stage of switches is required. These two switches must operate in a similar manner at a frequency of $F_S/4$ and with a phase difference of 90 deg. This basic approach has been demonstrated for the case of 1:4 demultiplexing of an optical signal carrying 16 Gb/s (ref. 2-6). For the general case of $M=2^N$

output ports, M-1 separate switches are combined in N stages. Switch arrays of 1x8 are possible using a single $LiNbO_3$ substrate, but larger arrays would require multiple substrates.

Our four-channel test system used a one-input, four-output lithium niobate ($LiNbO_3$) switch array, which was supplied to us by Hoechst Celanese (and fabricated by GEC Marconi). The insertion loss from the input fiber pigtail to a switch-selected output fiber varies between 8.1 and 11.9 dB for the different channels. This variation results from an error in processing, and lower, more uniform, insertion losses are expected to be quite possible. The optical power that leaks through to any of the unselected outputs was at least 18 dB below the selected output channel for all the various permutations. This is somewhat worse than the DC extinction ratios, which were better than 20 dB for all channels using the same switch array and the same pulsed laser. This difference is attributed to the finite width of the pulses combined with the sinusoidal waveforms that drive the switches. The consequence of crosstalk between channels in the performance of the HOE-ADC is to alter the system frequency response. It is equivalent to inserting a finite-impulse response filter, and, because this operation is linear, no distortion is introduced.

2.2.4 Electrical Drive Circuitry

The switch array was supplied from Hoechst Celanese in a hermetically sealed 56-pin DIP package. We designed an alumina PC board and mounting hardware that supplied all bias connections via a ribbon cable connection and SMA connectors and 50Ω waveguides for the RF inputs. Each switch has three control voltage inputs that adjust the interferometer bias and the splitting ratio of the input and output directional couplers. These tuning voltages are set under computer control, and, as the RF inputs are of a constant power level, there is no significant drift in the optimal control voltage settings over time periods of days.

The switching voltages from 50Ω sources for these switches are 10.6V for the one that runs at 1 GHz and 8.4V for the switches that run at 500 MHz. The circuitry that supplies the RF inputs to these switches, as well as a synchronous drive signal for the laser and the electronic A/D clock input, is shown in figure 2-3. The output from an HP 8657B synthesized signal generator (which is bandfiltered to remove subharmonics) serves as the master clock that drives the pulsed laser at 2 GHz. This signal is frequency divided by using a GaAs T-type flipflop (NEC model UPG701B). The 1-GHz output from this device is sent to the first-tier switch and to a second identical T-type flipflop. This chip generates a 500-MHz signal used to drive the two second-tier switches and the clock for the electronic sampler. The variable attenuators are used to separately adjust the amplitudes of the sinewave drives. The phase adjustments indicated in the different output lines were made by trimming the coaxial cables to appropriate lengths.

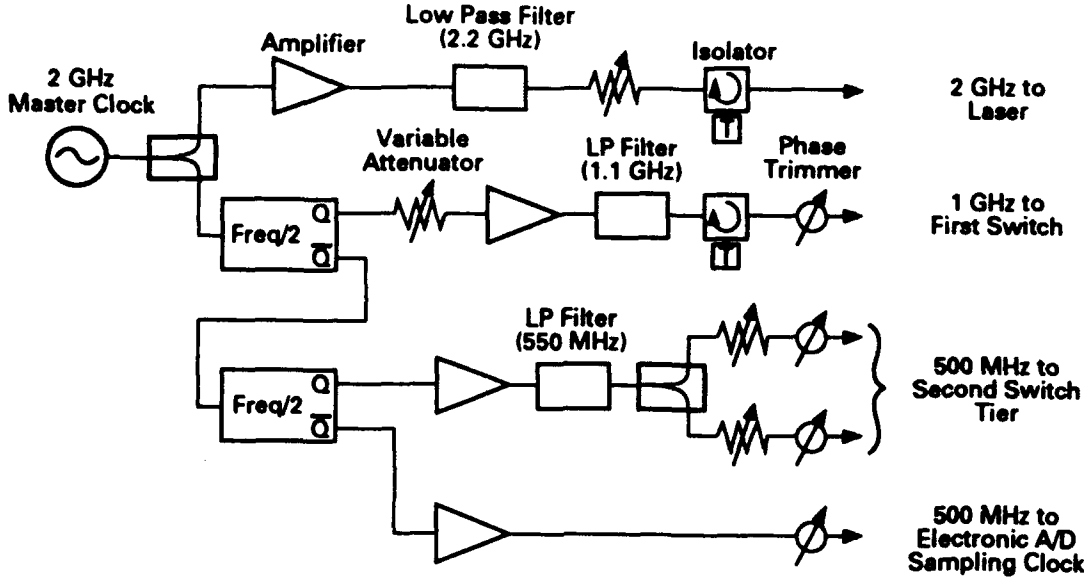

Figure 2-3. Switch Drive and Synchronization Electronics

2.2.5 Optical Switch Array Alignment Procedure

To minimize the crosstalk between channels, each switch should be driven at an optimal amplitude, bias, and phase. Because the optical pulses do have a significant width, the lowest crosstalk is obtained when the pulses are concurrent with the voltage maximums or minimums. A significant advantage of the gain-switched laser was that we could drive it at almost arbitrary frequencies so long as a source of short electrical pulses was available. Using a 500-MHz step-recovery diode driven by a separate synthesized signal generator that was phase-locked to the generator used to drive the switch array, we produced 500-MHz optical pulses. The phase relationship between these generators was variable and was set under computer control while performing the alignment. First taking note of the phase of the 2-GHz laser pulses by using the sampling oscilloscope, the laser was shifted to the 500-MHz drive setup and phase-adjusted to match the original pulse timing. This setup allowed the light from the laser to be directed to any one of the four output ports by selecting an appropriate phase shift. Leakage into unselected channels was minimized by iteratively adjusting the switch-drive parameters.

2.2.6 Fiber Interconnections

Optical interconnections between the separate components of the HOE-ADC test system were all made using single-mode optical fiber. Because the $LiNbO_3$ devices are polarization dependent, we had to ensure the polarization was optimal for light entering both the modulator and the switch array. The modulator was purchased with polarization-preserving fiber pigtails for input and output. Between the laser and the input to the modulator, there is a GEC-supplied polarization controller that can transform any input polarization state to a specific output. Adjustments were made to this device to maximize the modulator throughput; we empirically found that this simultaneously maximized the

modulator contrast. To help overcome some of the switch-array excess loss that resulted from fabrication error by GEC, we had GEC fusion-splice the polarization-preserving fiber input to the switch array to the modulator output. This splice introduces only ≈0.1 dB of loss and is rotationally aligned to maintain proper polarization. The four output fiber pigtails from the switch array were connected to input fiber pigtails to the optical receivers. For the exception of the fusion splice, fiber connections were made by using standard FC/PC connectors.

For convenient system testing we arranged our components with large separations. In a packaged system, a much smaller volume and shorter lengths of fiber could be used. However, it is important not to inadvertently give up immunity to EMI, which is characteristic of optical-fiber connections, by locating components too closely together.

2.2.7 Optical Receivers

Each of the output fibers from the switch array is sent to a detector where the light pulses are converted to electrical pulses with a peak voltage proportional to the optical pulse energy. Time-demultiplexing allows the bandwidth of the detector and the following electronics to be reduced from the bandwidth of the sampling process. This results in the electrical pulse width becoming broad compared with the optical pulse width. To avoid temporal crosstalk between successive pulses, the broadening must be limited so that the electrical pulses do not significantly overlap during the sampling aperture of the electronic A/D converter.

Our detectors were PIN-FET receiver modules with a bandwidth of roughly 700 MHz that were obtained from Lasertron (model QDFH). These fiber-pigtailed packages had a responsivity greater than 0.8 A/W at our 1,300-nm wavelength and an electrical gain of roughly 10 dB. An additional electrical gain of 30 dB was obtained using low-noise, 10- to 1,500-MHz-bandwidth amplifiers (Mini-Circuits model ZFL-1000H).

2.2.8 Electronic Digitizers

The electronic A/D converters that sample the received pulses must operate synchronously with the demultiplexed pulse rate and be phased so that sampling takes place near the peak of the electrical pulses. We found that the fastest commercially available A/D converters were obtainable in the form of digital oscilloscopes. These instruments typically contain A/D converter circuits that are internally clocked; no provision is made for external access to this clock. In a packaged system, an investment would be required to package a set of custom-supplied A/D converters, together with an external clock input, and fast digital memory. For the purpose of building our HOE-ADC test system, however, we were constrained to use existing digitizing instruments.

Analytek System

We primarily used an instrument obtained from Analytek consisting of four A/D converters capable of operating in parallel. Unlike most digitizer manufacturers, Analytek did give the user provision

to use an external clock. A 500-MHz signal derived from the 2-GHz laser drive was sent to this system to act as a sampling clock for all of the input channels. Each channel has a 3-dB bandwidth of 350 MHz, which is somewhat higher than the 250-MHz Nyquist bandwidth required for our 500-MHz sampling rate. This system is capable of recording 8,192 consecutive samples, corresponding to a record length of roughly 4 μs.

It is important to note that the precision of the electronic digitizer when used in the HOE-ADC is not typically contained within the manufacturer's specifications. This results from the pulsed electrical waveform from the receivers having spectral content above the Nyquist sampling rate. For example, jitter in the sampling process within the digitizer causes more severe errors for our pulsed input signals than for a signal strictly limited to the Nyquist band. The Analytek instrument performed an internal 1x8 demultiplexing for each of the input channels. The slightly varying time delay to these separate channels caused a systematic "jitter" that reduced the system precision. To be fair to this instrument manufacturer, it is important to note that the pulsed signals we are sampling contain frequency components that are above the rated bandwidth of the instrument. It performs with considerably higher precision (at least 4.5 effective bits) for single-tone inputs at frequencies below 250 MHz. With our experience, it is clear that a preferred approach is to perform the sampling before demultiplexing (this method is used by Hewlett-Packard in their digitizing oscilloscopes).

Hewlett-Packard System

The other electronic digitizer we used was a Hewlett-Packard 54111D digitizing oscilloscope. This instrument does not possess some of the systematic problems that the Analytek system has and has performed with slightly better precision for our application (further description of these points is deferred to section 5.0). It served as a helpful diagnostic tool, but as only one channel could be sampled with this oscilloscope, our full system demonstration relied on the four-channel Analytek instrument. Like the Analytek instrument, this system is also capable of recording 8,192 consecutive samples, corresponding to a record length of roughly 16 μs. Because this oscilloscope has an internal clock with no outside access, we had to match the laser pulse rate to the fourth-harmonic of the sample rate. This could be done quite accurately (to within about 10 Hz), and during the 16-μs record, drift between the two clocks was negligable. However, while taking measurements, it was necessary to wait for the proper clock phase.

2.3 Factors Limiting Performance

The precision of the HOE-ADC is limited by a combination of noise sources and systematic errors that result from distortion, crosstalk, and quantization. In this section we attempt to identify the primary sources of error and provide analysis relating the magnitude of these sources to the various system parameters. To simplify comparison among the different error sources, they are expressed as SNRs.

A standard method of characterizing the precision of A/D converters is based on converting a measured SNR to a number of "effective bits," which is the number of bits required for an ideal

A/D converter having the same SNR. For an ideal A/D converter with 2^N equally spaced levels separated by voltage increments of V_Q, the standard deviation of the quantizing errors resulting from a sequence of samples, which are distributed uniformly in voltage, is $V_Q/\sqrt{12}$. The resulting SNR due to quantization of a full-scale sinusoidal signal is

$$(SNR)_Q = 6\left(2^{N-1}\right)^2. \tag{2-4}$$

The number of effective bits is defined by solving the previous equation for N to yield:

$$N_{effect} \cong \frac{(SNR)_{dB} - 1.76}{6.02} \tag{2-5}$$

where $(SNR)_{dB}$ is the measured SNR expressed in decibels.

Several of the significant error sources result from the pulsed laser having limited power and stability; namely, shot noise, pulse-timing fluctuations, and pulse-energy fluctuations. Additionally, noise is introduced within the detection electronics and the digitizing process. Expressions are developed for these various noise sources in this section. We have found that some of these expressions have characteristic dependence on the phase of an applied sine-wave test signal. This phase dependence of the noise power has proved to be a powerful diagnostic in determining the relative levels of the separate noise sources.

2.3.1 Shot Noise

Where shot noise is the sole source of error, if the mean number of detected photoelectrons from a pulse is n, then the uncertainty of this quantity is $\sqrt{n}$. It is important to note that to apply this same uncertainty to the sampled peak-voltage of a pulse from the receiver, there must be significant pulse broadening to effectively time integrate over the duration of the optical pulse. If a modulator with the transfer characteristic of equation 2-1 is used and is driven sinusoidally about the inflection point, then n is given by:

$$n(\theta) = \frac{\eta \Gamma E_p \lambda}{2hc}\left[1 + \sin\left(\frac{\pi V \sin(\theta)}{V_\pi}\right)\right] \tag{2-6}$$

where η is the detector quantum efficiency, Γ is the optical transmission, E_p is the laser pulse energy, λ is the laser wavelength, h is Planck's constant, c is the speed of light, V_π is the modulator switching voltage, V is the amplitude of the applied voltage, and $\theta = \omega t$ is the phase. The electrical power following detection is proportional to the squared photocurrent averaged over time and from equation 2-6:

$$\begin{aligned} \langle n^2 \rangle &= \langle n^2 \rangle_{DC} + \langle n^2 \rangle_{AC} \\ &= \langle n^2 \rangle_{DC} + \left(\frac{\eta \Gamma E_p \lambda}{2hc}\right)^2 \frac{1}{2\pi}\int_0^{2\pi} \sin^2\left(\frac{\pi V \sin\theta}{V_\pi}\right) d\theta \end{aligned} \tag{2-7}$$

where $\langle n^2 \rangle_{DC}$ is a term resulting from the DC bias of the pulses and does not constitute part of the desired signal. The AC electrical power that we associate with the desired signal can be expressed by evaluating the integral in equation 2-7:

$$\langle n^2 \rangle_{AC} = \left(\frac{\eta \Gamma E_p \lambda}{2hc}\right)^2 \frac{1}{2}\left[1 - J_0(2\sin^{-1} m)\right]$$
$$\cong \frac{m^2}{2}\left(\frac{\eta \Gamma E_p \lambda}{2hc}\right)^2 \qquad (2\text{-}8)$$

where J_0 is the zero-order Bessel function, $m = \sin(\pi V/V_\pi)$ is the modulation index from equation 2-2, and the approximation is good for $m << 1$. We now introduce the term "power phase density", or PPD, which is analogous to the more commonly used term, power spectral density. In the present context, we define the relative shot noise PPD to be:

$$PPD_{SHOT} = \frac{n(\theta)}{2\pi \langle n^2 \rangle_{AC}}$$
$$\cong \frac{2hc}{\pi m^2 \eta \Gamma E_p \lambda}\left[1 + m \sin\theta\right] \qquad (2\text{-}9)$$

This quantity is the amount of electrical shot noise power per radian of signal phase relative to the AC signal power. By integrating this density over the full range of signal phase, the shot noise limited SNR is obtained:

$$[SNR_{SHOT}]^{-1} = \int_0^{2\pi} PPD_{SHOT}(\theta)\, d\theta \cong \frac{4hc}{m^2 \eta \Gamma E_p \lambda} \qquad (2\text{-}10)$$

2.3.2 Laser Pulse-Energy Fluctuations

A similar analysis can be applied to pulse-energy fluctuations caused by relative intensity noise (RIN) from the laser. Similar to equation 2-6, we express the signal voltage following detection as:

$$S(\theta) = \frac{gE_p}{2}\left[1 + \sin\left(\frac{\pi V \sin(\theta)}{V_\pi}\right)\right] \qquad (2\text{-}11)$$

where E_p is now the *average* laser pulse energy and g is a constant. Again, considering only the AC component of the signal, the electrical signal power is proportional to:

$$\langle S_{AC}^2 \rangle = \left(\frac{gE_p}{2}\right)^2 \frac{1}{2\pi}\int_0^{2\pi} \sin^2\left(\frac{\pi V \sin(\theta)}{V_\pi}\right) d\theta$$

$$= \frac{(gE_p)^2}{8}\left[1 - J_0\left(\frac{2\pi V}{V_\pi}\right)\right]$$

$$\cong \frac{(mgE_p)^2}{8} \qquad (2\text{-}12)$$

If we assume that the pulse energy fluctuations arise from a normal distribution with a standard deviation of δE_p, then the resulting time-averaged noise power is proportional to:

$$\langle \delta S_{RIN}^2 \rangle = \left(\frac{g\delta E_p}{2}\right)^2 \left[1 + \sin\left(\frac{\pi V_0 \sin\theta}{V_\pi}\right)\right]^2 . \qquad (2\text{-}13)$$

Analogous to equation 2-9, the relative power phase density resulting from laser RIN is given by:

$$PPD_{RIN} = \frac{\langle \delta S_{RIN}^2 \rangle}{2\pi \langle S_{AC}^2 \rangle} \cong 2\left(\frac{\delta E_p}{mE_p}\right)^2 \frac{1}{2\pi}(1 + m\sin\theta)^2 \qquad (2\text{-}14)$$

and upon integrating this expression we obtain the RIN limited SNR:

$$[SNR_{RIN}]^{-1} \cong (2 + m^2)\left(\frac{\delta E_p}{m E_p}\right)^2 . \qquad (2\text{-}15)$$

2.3.3 Laser Pulse Jitter

The error in a detected sample voltage that results from a pulse timing error, $\delta\tau$, is given by:

$$\delta S_{JITTER} = \frac{gE_p}{2}\left\{\sin\left(\frac{\pi V \sin(\omega[t + \delta\tau])}{V_\pi}\right) - \sin\left(\frac{\pi V \sin(\omega t)}{V_\pi}\right)\right\} . \qquad (2\text{-}16)$$

Assuming a small-amplitude drive signal, small-angle approximations yield:

$$\delta S_{JITTER} \cong \frac{gE_p m\omega\delta\tau}{2}\cos(\theta) \qquad (2\text{-}17)$$

where $\theta = \omega t$ is the phase of the driving sine wave. If $\delta\tau$ is now regarded as the standard deviation from a normal distribution of pulse-timing fluctuations, or the pulse jitter, the relative power phase density is given by:

$$PPD_{JITTER} = \frac{\langle \delta S^2_{JITTER} \rangle}{2\pi \langle S^2_{AC} \rangle}$$

$$\equiv \frac{1}{\pi}\left[2 \cos\theta \sin\left(\frac{\omega\delta\tau}{2}\right)\right]^2$$

$$= \frac{1}{\pi}[\omega\delta\tau \cos\theta]^2 \qquad (2\text{-}18)$$

At this point the justification for introducing the concept of power phase density becomes apparent. By comparing equations 2-14 and 2-18, it is clear that the noise contributions originating from laser RIN and the timing jitter are distinguishable if the signal phase dependence of the noise is known. This characteristic is exploited in the following sections of this report in order to quantify the individual noise levels. In practice, the phase dependence of shot noise, given by equation 2-9, is indistinguishable from laser RIN. This is not a serious problem, however, as the level of shot noise is readily determined by the average detector photocurrent.

Again integrating equation 2-18 over signal phase, we can obtain the jitter limited SNR:

$$[SNR_{JITTER}]^{-1} = (\omega\delta\tau)^2 . \qquad (2\text{-}19)$$

2.3.4 Receiver and Amplifier Noise

The final noise source considered here is the electrical noise due to the receiver, amplifier, and electronic A/D converter. For our purposes, we lump the combined effect of these components into a single "noise-equivalent" power, P_{NE}, which represents the average optical power required at a single receiver to produce an SNR of unity. Thus, the value of P_{NE} is dependent on many factors, on which we do not elaborate. However, by defining this quantity, the dependence of the resulting receiver-noise-limited SNR on parameters we have already introduced is shown to be:

$$[SNR_{REC}]^{-1} = \frac{P^2_{NE}}{\left(\frac{\Gamma E_p f_s}{8M}\right)^2 [1 - J_0(2\sin^{-1} m)]}$$

$$\equiv 8\left(\frac{MP_{NE}}{\Gamma E_p f_s m}\right)^2 \qquad (2\text{-}20)$$

where M is the demultiplexing ratio and f_s is the sample frequency.

The noise given by equation 2-20 is only an approximation to the various noise sources encountered between detection and digitization. It may be able to accurately account for amplifier thermal noise: however, it does not include effects caused by sampling jitter that may take place within the electronic digitizer. This, and perhaps other noise sources within the amplifiers and digitizers, are beyond the scope of this report.

If the various noise sources discussed in this section are statistically independent, the noise power from each simply adds to the total noise power. Therefore, the overall SNR, limited only by the contributions of noise presented above, is given by:

$$SNR_{TOTAL} = \left([SNR_{SHOT}]^{-1} + [SNR_{RIN}]^{-1} + [SNR_{JITTER}]^{-1} + [SNR_{REC}]^{-1} \right)^{-1} . \quad (2\text{-}21)$$

2.3.5 Systematic Errors

Distinct from the noise errors just described are several mechanisms in the HOE-ADC system that produce deterministic errors. These errors can be categorized as distortion, cross-talk, channel mismatch, and quantization "noise." For simple input signals, such as a single tone, all of the noise errors discussed previously produce a uniform white-noise background in the power spectrum. In the case of systematic errors, however, the power spectrum is corrupted with isolated "spurs," or, in the case of crosstalk, variations are produced in the frequency response. Another distinguishing feature of the systematic errors is that, (for the exception of quantization effects), the recorded samples can in principle be corrected to cancel their effect. This feature was exploited in our demonstration system in the case of channel mismatch. As mentioned in section 2.4, the gain and offset levels of each channel are not critically matched until after the sampled data are processed by the laboratory computer.

2.4 Four-Channel HOE-ADC System Characterization

Connecting the various components described in the previous section was simplified by the entire optical signal path being confined to fiber or waveguides. However, for the system to function in the intended manner, a somewhat tedious alignment process was required which involved cutting many of the coaxial RF lines to a set length and setting various control voltages and RF power levels so that the switch array and modulator functioned optimally. A laboratory computer was used for supplying the DC control voltages by way of D/A converters and also for acquiring the digitized information from the memory of the electronic digitizers to carry out several online tests to gauge system performance.

The modulator input signal was supplied by a synthesized microwave generator, which was phase locked with the generator supplying the 2-GHz drive for the laser. The signal was followed by a 6- to 18-GHz power amplifier, which could supply up to 1W, and the output was then bandpass filtered to 9.5- to 11.5-GHz to avoid harmonic distortion. A circulator was placed in the connection between the filter and modulator so that any reflected power would be absorbed and would reduce standing-wave effects in the frequency response.

Because of variations in optical throughput and electrical response among the separate channels, some method of relative calibration is required so that the sampled signal can be reconstructed. For a system to operate with a fast throughput, this operation would best be accomplished by making fine adjustments to the amplifier gains and offsets in each channel. While testing our demonstration system, a slow throughput was acceptable, and it was more convenient to perform normalization of the channels digitally. Initially, a signal was applied at a set calibration frequency and a least squares fit to a sinusoidal was performed using the digital samples from each channel separately. The amplitude and offset coefficients determined by this computation were then used for gain and offset correction of samples obtained from subsequent acquisitions.

2.4.1 Sine Wave Testing in 10- to 11-GHz Band

Four-Channel Operation

Figure 2-4 shows a brief portion of a typical sample sequence obtained from our four-channel HOE-ADC system. The sinusoidal input signal had a frequency of 10.2675 GHz, and there are slightly more than five periods between sample points which are separated by 0.5 ns. The sine wave indicated in the figure thus represents a downshifted frequency of 267.5 MHz. The same least squares fitting technique used for channel normalization was also applied to this reconstructed waveform to determine the error for each sample. These errors, combined with the amplitude of the fitted sine wave, allow the noise power and signal power to be calculated separately. For this particular acquisition, the resulting SNR was determined to be 18.5 dB, or by application of equation 2-5, there were 2.78 effective bits.

The 4-μs record that is shown partially in figure 2-4 was Fourier transformed, and the power spectrum was calculated to determine the spectral distribution of the errors. As seen in figure 2-5, there are many spurs in the presence of a uniform noise background. These spurs account for roughly half of the noise power with the largest at a level of -32 dBc. The cause of these discrete error components in frequency space is attributed to systematic effects in the sampling process that is used by the Analytek instrument (see sec. 2.2).

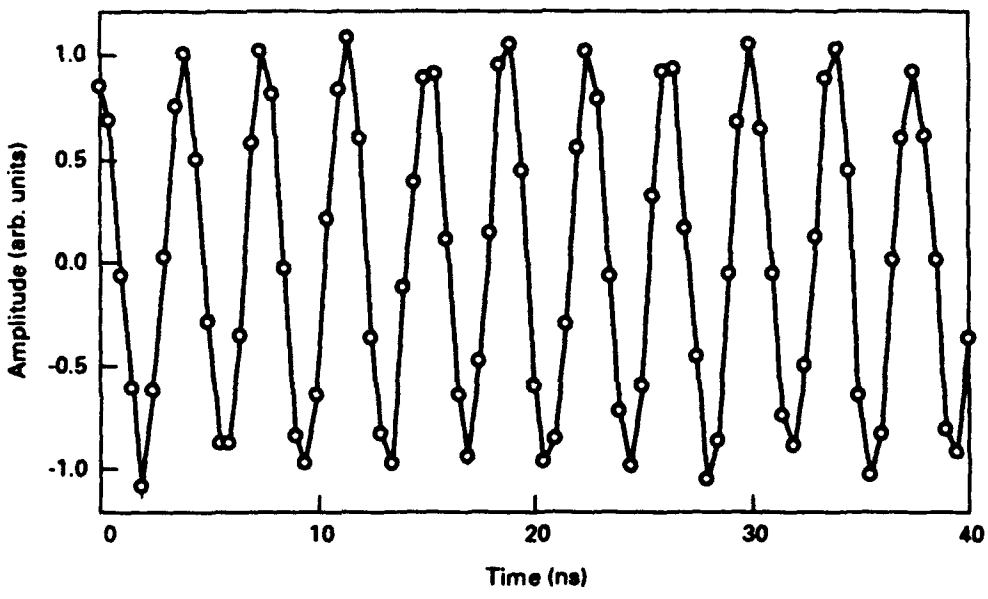

Figure 2-4. Reconstructed 10.2675 GHz Signal From 4-Channel HOE-ADC

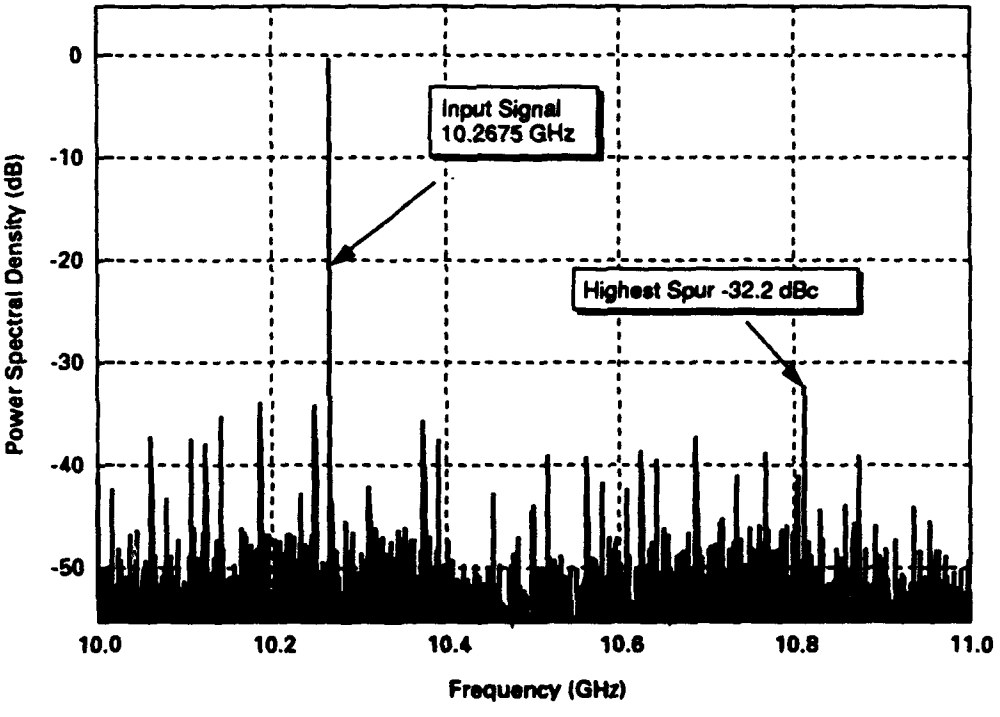

Figure 2-5. Power Spectral Density of Typical Digitized Waveform

Measurement of Frequency Response

By interfacing the computer to the signal generator, we performed a stepped measurement of the frequency response of this system over the desired 10- to 11-GHz band. After first performing the channel normalization at a frequency of 10.57 GHz, an acquisition was obtained at intervals of

2.5 MHz to determine the signal power and the SNR; these results are shown in figure 2-6. Unusual features of the frequency response are the falloff at 10 and 11 GHz and the notch at 10.5 GHz. These characteristics are due to the signal being AC coupled between the detectors and the inputs to the electronic A/D converters. The width of the notch is roughly 20 MHz and is consistent with the 10-MHz cutoff of the amplifiers we used. By using DC coupling of the signal after detection, these effects could be avoided. The other variations in response across the band are at a level of roughly ±1 dB and are attributed to the ripple associated with the modulator, modulator drive amplifier, and receiver electronics.

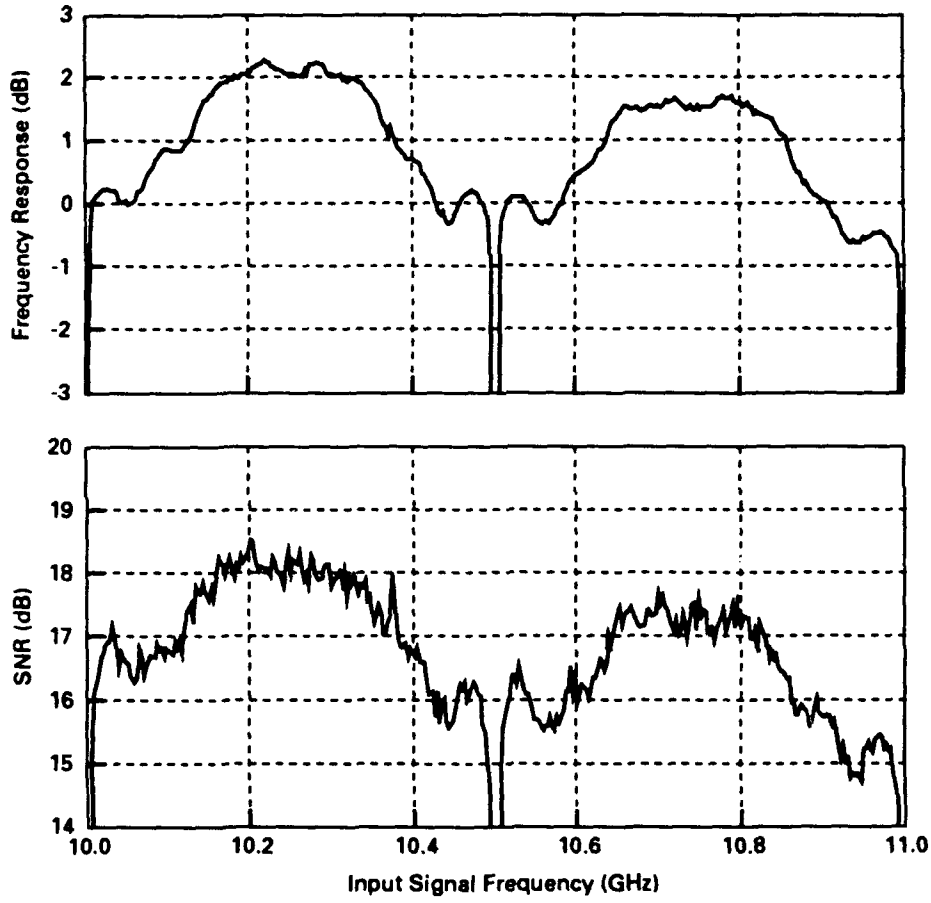

Figure 2-6. System Frequency Response and SNR for 10- to 11-GHz Band

Single-Channel Operation

Some of our testing was done using only one output channel and with electrical A/D conversion performed by the Hewlett-Packard digitizing oscilloscope. Because this instrument provides no convenient means to access its internal sampling clock, we could not phase-lock the light pulses to the electrical sampling. However, we were able to set the laser frequency to be synchronous with the sampling rate to within roughly 10 Hz, and the phase drift over a 16-μs acquisition period was negligible. A good record of samples in which the phases of these two oscillators were sufficiently close together could then be obtained by repeatedly acquiring data until the detected samples

exceeded some threshold level. Figure 2-7 shows a power spectrum of a sample sequence obtained by this method with the use of an input signal frequency of 10.033 GHz. The frequency axis in this plot covers the baseband Nyquist range, and the signal has been downshifted to 25.4 MHz. The only significant spurs in the spectrum result from downshifting the second and third harmonics of the signal to the baseband at 50.7 and 76.1 MHz.

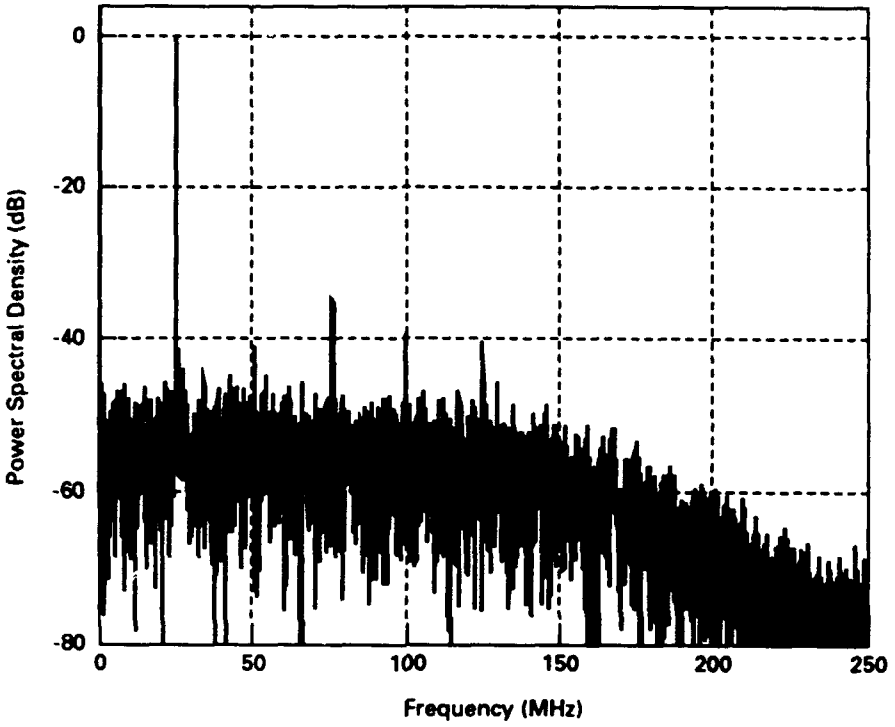

Figure 2-7. Power Spectrum From One-Channel Test, f = 10.033 GHz

Long after the measurement described above was performed, we realized that a digital filter within the Hewlett-Packard digitizing oscilloscope had inadvertently been enabled when these data were acquired. The resulting low-pass filter accounts for the frequency rolloff shown in figure 2-7 and led to the noise being underestimated. Assuming the actual noise distribution to be essentially white, the direct SNR measurement accounts for roughly 60% of the noise power. After correcting for this effect, this record had a precision of 3.0 effective bits. The cause for improvement over the results mentioned earlier is divided between the reduction in systematic sampling errors, (i.e., there are fewer spurs) and the use of the output channel with minimum optical loss.

Phase Dependence of Noise To Determine Pulse Jitter

The noise-power contributions due to shot noise, laser RIN, and laser pulse jitter are each dependent on the signal phase as previously shown in equations 2-9, 2-14, and 2-18 respectively. The distinction of the phase dependence between shot noise and laser RIN is quite slight, and quantifying them separately on this basis alone would require very accurate measurements. However, the noise power, which is due to pulse jitter, is quite distinct from the phase dependence of the other noise sources. Qualitatively, we note that the jitter noise is a maximum at the two inflection points of the signal drive

cycle, the points where the signal is changing the fastest. This is easily separable from the noise of the other sources, which are a maximum at the point in the drive cycle where the modulator transmission is highest.

A sampled waveform obtained from a single channel of the HOE-ADC system (the same one used for preparing the power spectrum of figure 2-7) was used to determine the magnitude of the pulse jitter following the approach outlined above. To measure the phase dependence of the noise, a least squares fit to a sine wave was first performed. There was a slight systematic phase dependence of the residuals of the fit caused by the the harmonic spurs, which are evident in figure 2-5. To eliminate this systematic error, we included two extra sinusoidal components in the fit, which corresponded to the second and third harmonics of the signal. Following this fit, the phase of the drive fundamental can be determined at each sample time. The sample values from this data set are plotted in figure 2-8 versus the sine-wave phase. The data points are grouped within horizontal lines simply because the Hewlett-Packard digitizing oscilloscope uses a 6-bit A/D converter, and there are 128 discreet levels spanning the full-scale range. The residuals are obtained by subtracting the sampled values from the calculated fit and are plotted in figure 2-9. The curved groups of points in this plot are artifacts of the quantized levels, and if one ignores this distracting feature, it is apparent that the residuals tend to be larger in the phase regions centered at 0 and 180 deg. Using these residuals, the noise power phase density was calculated relative to the signal power and is plotted in figure 2-10, (after first averaging these values over 10-deg segments of signal phase). To correct for the unintentional filtering mentioned above, the measurements of power phase density in this figure have been increased by 67%. The dominant phase dependence of the noise in these data is a result of pulse jitter because there are two peaks in this plot close to the inflection points of the drive signal. A fit to these data was performed using a function of the form $A + B\cos^2(\theta)$ where A and B are constants. The resulting best fit is plotted as a solid curve on top of the data points in figure 2-10. The value of B represents the noise contribution due to jitter, and applying equation2-18, we determine the RMS pulse jitter to be 1.2 ps. This is in reasonable agreement with the 1.7-ps measurement of jitter mentioned in section 2.2 when considering that both techniques are of modest accuracy.

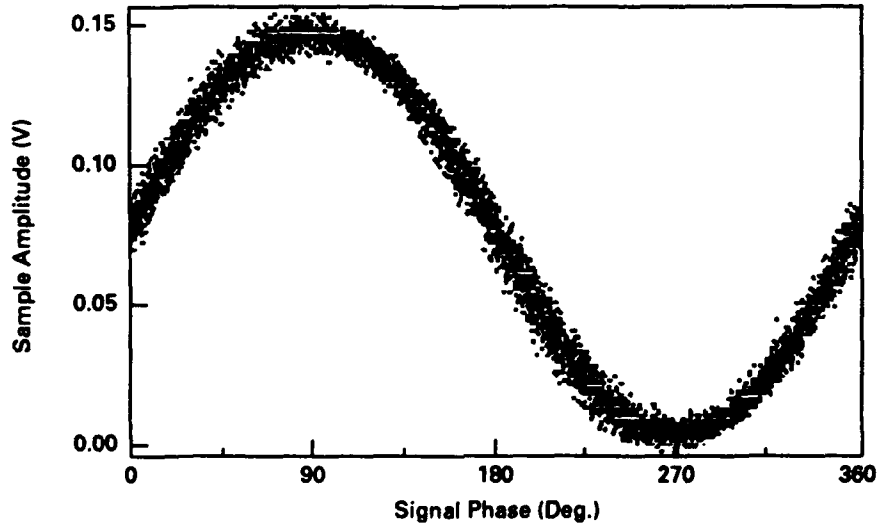

Figure 2-8. Sampled Data Versus Signal Phase, f = 10.033 GHz

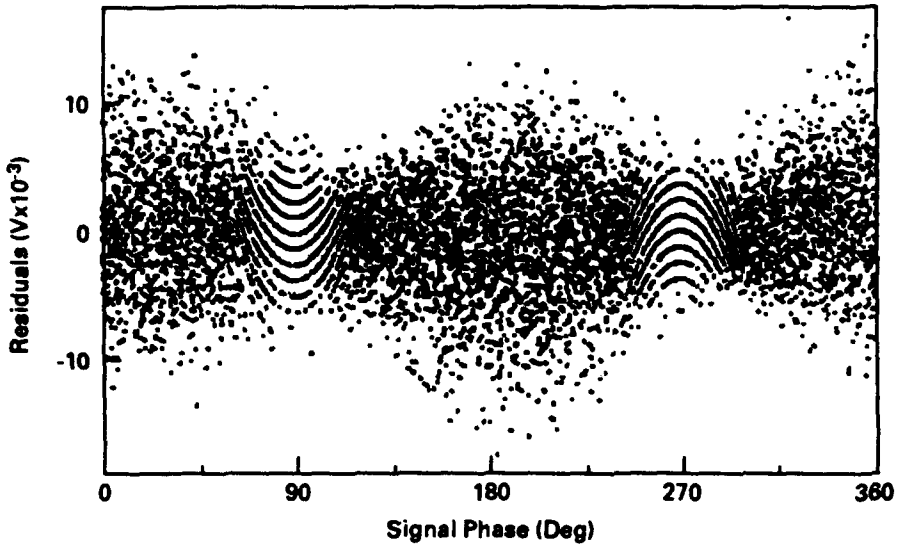

Figure 2-9. Residuals to Sine-Wave Fit Versus Signal Phase, f = 10.033 GHz

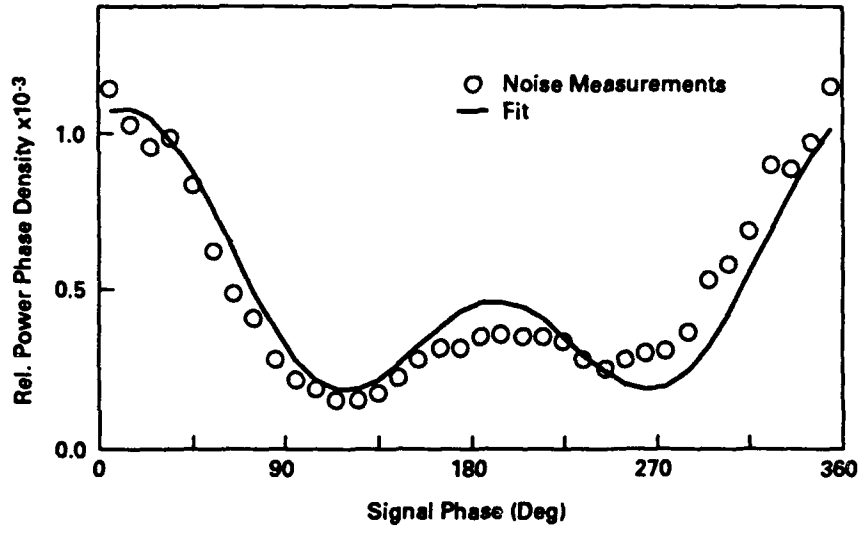

Figure 2-10. Relative Power Phase Density and Fit to Jitter-Induced Noise, f = 10-.033 GHz

2.4.2 Baseband Testing

We shifted our attention from the 10- to 11-GHz band down to the baseband to determine whether the resulting precision is consistent with our estimate of laser jitter. Also, to characterize system distortion, we performed a two-tone test, which we were unable to accomplish at the higher frequency for lack of a second microwave generator. During these tests, the amplifier driving the modulator was replaced with another that operated from 10 to 1000 MHz and had a 1-dB compression point of 31 dBm.

The two-tone measurements were carried out over a range of drive levels by using equal power tones at 291 and 293 MHz. We initially sent the electrical drive signal to a spectrum analyzer to verify that the third-order IMPs at 289 and 295 MHz were at least 65 dB below the power level of the intended tones. After going through the four-channel HOE-ADC system with this input signal, we again determined the level of the IMPs. Over the range of drive levels tested, we found these distortion products to vary between -25 and -38 dB relative to one of the input tones. These measurements were within 1 dB of the predicted distortion levels calculated from the nonlinear response of an ideal Mach-Zehnder modulator given in equation 2-2. As the distortion of the system was thus demonstrated to be largely accounted for by the nonlinearity of the modulator, a significant improvement could be realized by either (1) replacing the Mach-Zehnder modulator with a linearized modulator as discussed in section 2.2 or (2) implementing a distortion compensation technique, possibly by using the digitized samples as addresses to a lookup table.

The phase dependence of noise from a 243-MHz sine-wave dataset was analyzed in the same manner described in the previous section. These results are plotted in figure 2-11, and as expected, the jitter dependent contribution to this noise is much less for this low-frequency signal. Because this noise source was much reduced, we obtained a precision at this frequency of 3.7 effective bits – a gain of 0.7 bits over the jitter-limited result at 10.033 GHz. Also shown on this plot is a solid curve representing a fit to the expected noise from pulse-energy fluctions given by equation 2-14. The parameters of this fit, together with the measured modulation index of 0.75, provide an estimated variance of the pulse energy of 1.7%. It is important to note that these energy fluctions are not the limiting source of noise at baseband. As seen in figure 2-11, there is a substantial noise term that is independent of signal-phase angle that is attributable to receiver noise. Thus, even if the laser pulses were perfectly regular in energy, we would expect the noise power to decrease by only ≈ 25%. A significant gain in system performance at baseband is therefore dependent on both improving the laser stability and on increasing the light level at the receivers.

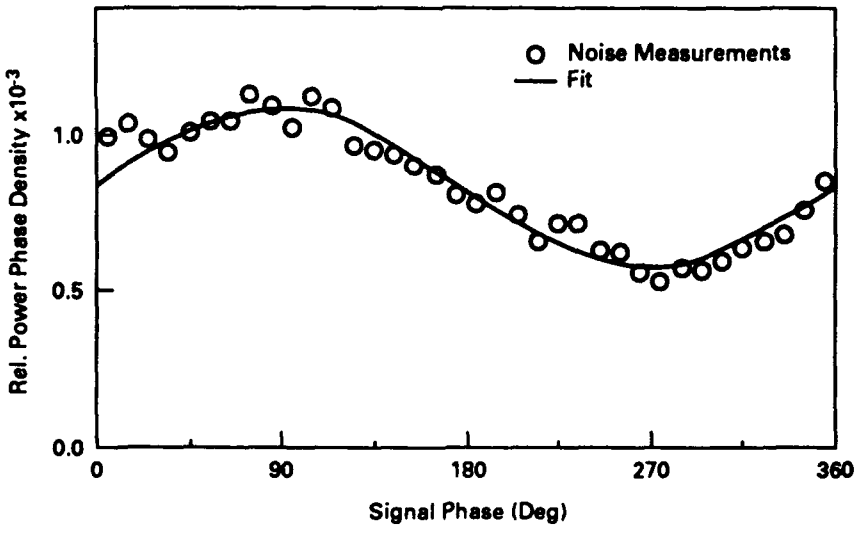

Figure 2-11. Relative Power Phase Density and Fit to RIN and Excess Noise, f = 243 MHz

3.0 DIGITAL SWITCH ARRAY DEVELOPMENT

Our strategy for improving the prototype HOE-ADC involved, in part, developing an improved switch array having lower insertion loss than the commercially obtained switch array. The commercial array had pigtailed insertion lossesranging from 9 to 12 dB in the four channels . Our objective with the replacement switch array was to reduce losses to about 5 dB. A novel feature of the new array was the use of digital optical waveguide switches, invented by Dr. Suwat Thaniyavarn of Boeing (ref. 3-1). These devices provide an extended region for low-crosstalk switching compared with conventional switches with sinusoidal response characteristics. This removes the necessity for precise setting of the drive voltage amplitudes. Because we have an excellent $LiNbO_3$ optical-waveguide fabrication capability at Boeing, we naturally chose that material system for implementing the switch array. Waveguides are made in this material by diffusion of thin-film titanium into the surface at approximately 1050°C. This reliably yields very low-loss, single-mode waveguides. The crystal orientation used in this program was z-cut because it allows lower losses in coupling to optical fibers. The remainder of this section describes the experiences and results in developing this new type of switch array.

3.1 Device Theory and Design

The structure of the 1x2 digital switch is shown in figure 3-1. It is based on a symmetrical 1x2 directional coupler with specially designed electrodes. The electrode structure consists of two sections of asymmetrical delta-ß phase reversal electrodes of unequal length. A digital switch response can be synthesized by proper choice of these two lengths. First, the overall interaction length must be twice the coupling length ($L=2\ell_c$). Second, the second electrode section must be slightly more than twice the length of the first section (i.e., $L_1/L = 0.68$ and $L_2/L = 0.32$). The intensity-versus-voltage transfer characteristic corresponding to these choices is shown in figure 3-2. Also shown is the transfer characteristic of a conventional directional coupler. It is obvious that the digital switch maintains low crosstalk over a much more extended drive voltage range. Thus, it is more robust in the presence of drifts in the drive level or bias.

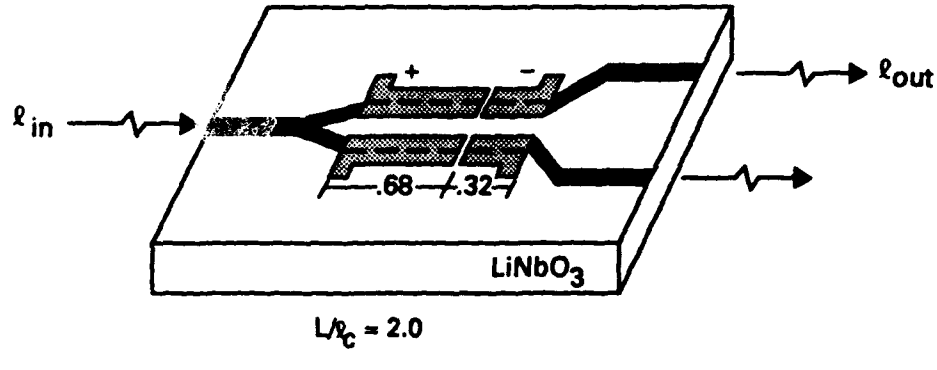

Figure 3-1. Schematic Design of the 1x2 Directional Digital Switch

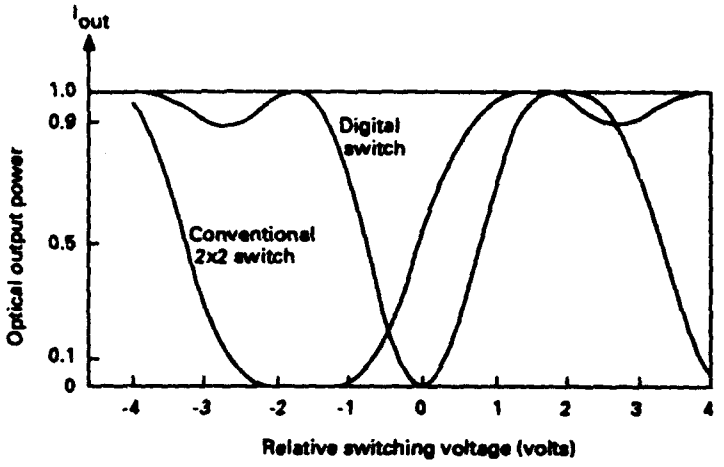

Figure 3-2. Intensity Versus Voltage Characteristic for the Digital Switch and a Conventional 1x2 Directional-Coupler Switch

Additional insight into the transfer characteristic of the digital switch can be had from its modulation diagram (fig. 3-3). The use of modulation diagrams in analyzing the performance of optical waveguide devices is discussed in reference 3-2. This diagram gives the contours of constant crosstalk as a function of the ratio L/ℓ_c and the drive voltage (proportional to delta-ß, the voltage-induced shift in the propagation constant). The dark, extended regions at $L/\ell_c=2$ correspond to crosstalk levels below -30 dB. The horizontal extent of these regions corresponds to a voltage range of about 10 times the range for -30-dB crosstalk in a conventional directional coupler. The key to the practical realization of this digital feature is tight control of the coupling length because, as shown in figure 3-3, the crosstalk degrades rapidly for deviations in L/ℓ_c from the value 2.

3.2 Optical Parameters for the Digital Switch

The first step necessary in developing the digital switch was to determine the relationship between the fabrication parameters and the resulting coupling length. We had previously demonstrated a DC response for a digital switch designed for an optical wavelength of 1,300 nm. To accommodate inclusion of a fiber-optic optical amplifier operating at 1,500 nm in the HOE-ADC, the basic measurements of the coupling length had to be repeated for the new wavelength. As discussed in the previous section, the digital characteristic exists only over a narrow range of values for L/ℓ_c. Because $LiNbO_3$ optical waveguide fabrication is not yet well standardized, the coupling length must be determined by tediously characterizing a number of devices whose design parameters are systematically varied. It was convenient, and sufficient, to use 2x2 directional couplers for this purpose. The result was to learn the specific waveguide width, gap, and coupling length that results in complete exchange of energy between either of the two inputs. For the fabrication conditions used (titanium thickness, diffusion temperature, and time), it was found that parallel waveguides with widths of 7 μm and a gap of 13.8 to 14.0 μm yielded a coupling length of 15 mm. A final round of fabrication experimentation was necessary to ensure that when oxide and metallization layers were added, the coupling length did not change. This was, in fact, found to be the case.

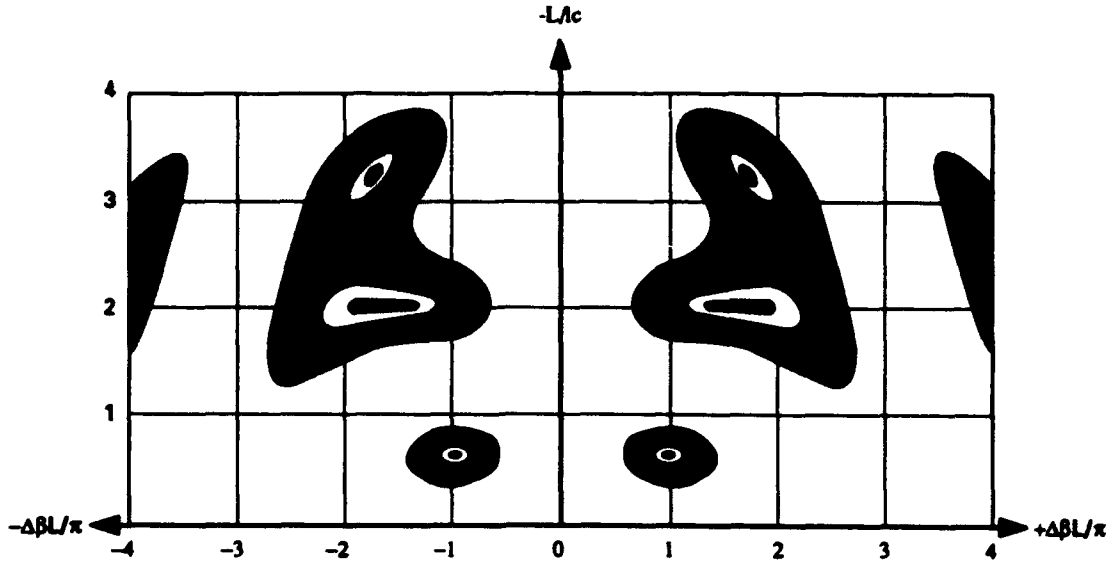

Figure 3-3. Modulation Diagram for the Digital Switch

3.3 First Prototype Digital Switch

For 4 GS/s operation of the HOE-ADC, the first-tier digital switch has to operate at 2 GHz. This is at the extreme upper end of feasibility for lumped-element electrodes. It was decided that, in spite of this, a lumped-element electrode approach offered a lower risk approach than a traveling-wave design, considering the schedule and funding constraints of the program. Transformer-coupled electrical matching was planned for enhancing the response at 2 GHz.

The next step in developing the 1,500-nm digital switch was to design the two-section electrodes. The length relationships have already been discussed. The lateral geometry and placement of the electrodes relative to the waveguides are also important for maximizing the efficiency. Our general approach was to seek an optimum design for maximizing the overlap of the optical and electrical fields for 1,500-nm light, while keeping the resistance, R, and capacitance, C, to values compatible with resonant tuning. Our first-generation device emphasized maximizing the overlap integral. The motivation was that the digital switch, compared with conventional switches, has a switching voltage that is about 1.5 times higher. (We define the switching voltage as the voltage range between the center of the fully switched on and off states). This higher switching voltage means a greater drive power by about a factor of 2. Also, operating at the longer optical wavelength of 1,500 nm would incur an additional small drive voltage penalty.

With our concern over switching voltage, a four-conductor electrode was chosen that would maximize the overlap integral. Using the previously measured coupling length, masks for waveguides and electrodes were designed and fabricated. Figure 3-4 shows top and cross-sectional views. Both thin-film (300 nm) aluminum and thick (4,000 nm) electroplated gold electrodes were used. In both cases, a 350-nm-thick SiO_2 buffer layer was deposited over the entire substrate surface. The purpose of the buffer is to isolate the optical fields from the electrodes and allow for redistribution of electrical charge generated by pyroelectrical effects. In the thin-film electrodes the indicated

interconnects between electrode sections were incorporated into the mask pattern. For the thick-film electrodes, ultrashort jumper wires were used. Though offering an enhanced overlap integral, there were two concerns associated with the four-conductor design. One was that the narrowness of the two interior conductors might cause excessively high resistance. The other was the degree of increased capacitance. It remained to be seen what actual penalties in capacitance and resistance would be incurred.

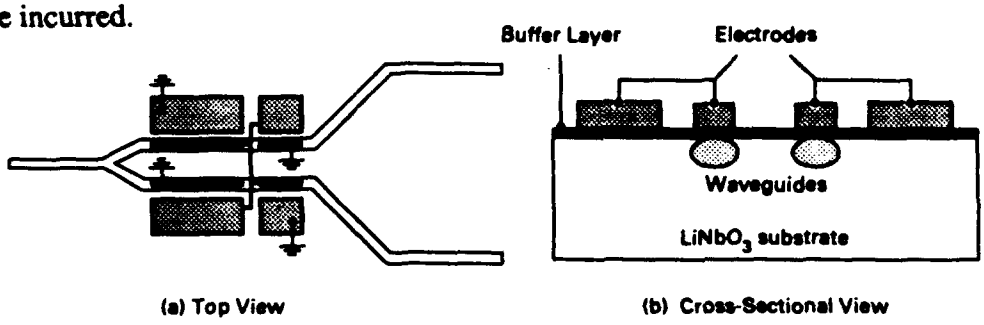

Figure 3-4. Four-Conductor Electrode Design for the First-Iteration Digital Switch

A set of devices were made on a common substrate that had a range of design parameters. These devices typically exhibited DC switching voltage values of about 10 volts. For these DC measurements, a single electrode served all devices on the substrate to facilitate evaluation of a large number of devices. However, the extremely large capacitance precludes high-frequency response measurements. A typical measurement of the transfer characteristic is shown in figure 3-5. The basic digital shape was exhibited but with a dimple of increased crosstalk at the fully switched position. This was attributed to nonnegligible coupling in the separation region at the device output. To fine-tune this aspect of the design, a family of devices was made with varying electrode lengths and coupling regions. Results for four different cases are shown in figure 3-6. The design with the flattest shape in the off states had a waveguide separation region equivalent to 1.5% of the overall coupling length.

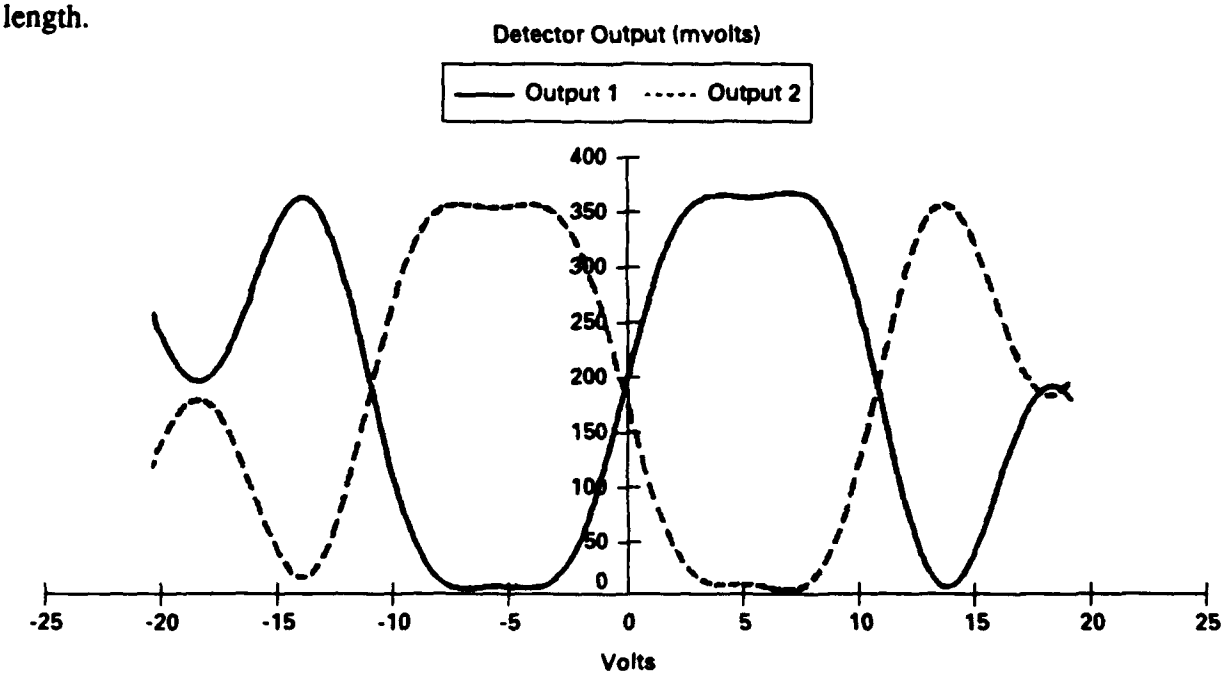

Figure 3-5. Measured Transfer Characteristic for a Four-Conductor Digital Switch

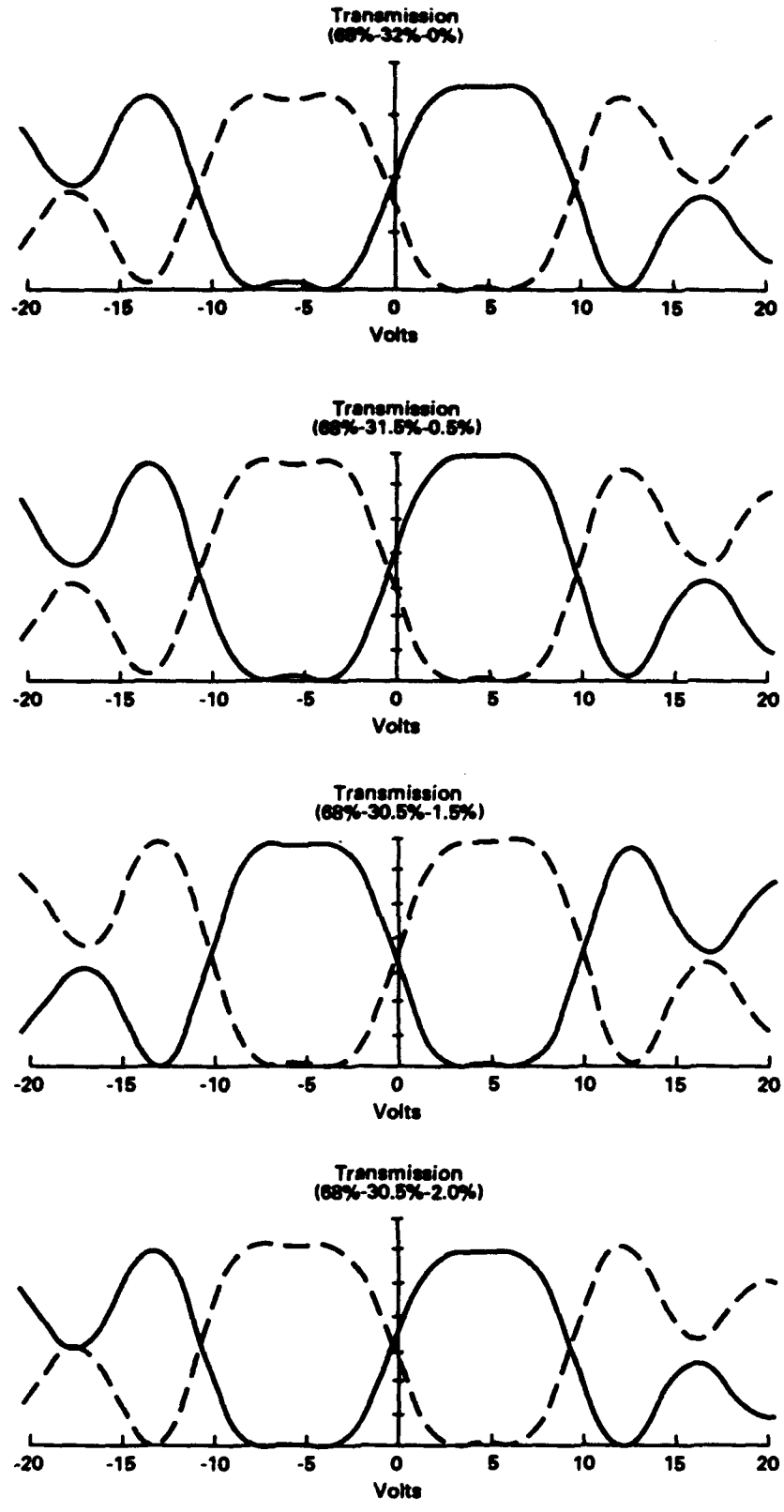

Figure 3-6. Transfer Characteristics for Four-Conductor Digital Switches With Small Differences in the Effective Length of the Waveguide Separation Region

With the DC characteristics optimized, a new electrode mask was designed that allowed individually addressable electrodes for each device to enable high-frequency testing. Unfortunately, the frequency response of these devices exhibited excessive rolloff, decreasing by 20 dB at 2 GHz because of higher than anticipated capacitance and resistance. Although an iteration of the design would have improved the result, we felt that the degree of improvement would not be sufficient to warrant the effort. Alternatively, it was decided to revert to a two-conductor design.

3.4 Two-Conductor Digital Switch

Top and cross-sectional views for a digital switch with a two-conductor, two-section electrode design are shown in figure 3-7. The two-conductor electrode has inherently less capacitance because there are two, rather than four, closely spaced conductors. The resistance is less because neither of the conductors is constrained to a narrow dimension. In the first two-conductor devices, the metallization and buffer layers were similar to those used for the four-conductor devices. A set of these devices was made and the DC switching characteristic measured. A typical result is shown in figure 3-8. It exhibits a switching voltage of 18V compared with about 10V for the four-conductor devices. Obviously, a drive power penalty would be paid for improving the speed.

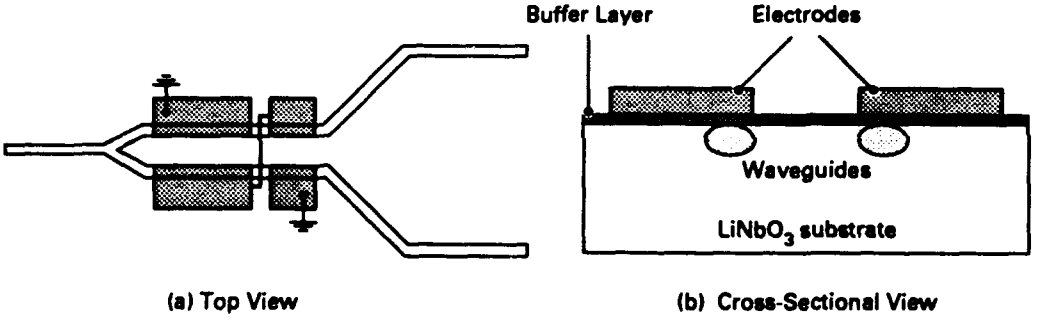

Figure 3-7. Two-Conductor Electrode Design for the Second-Iteration Digital Switch

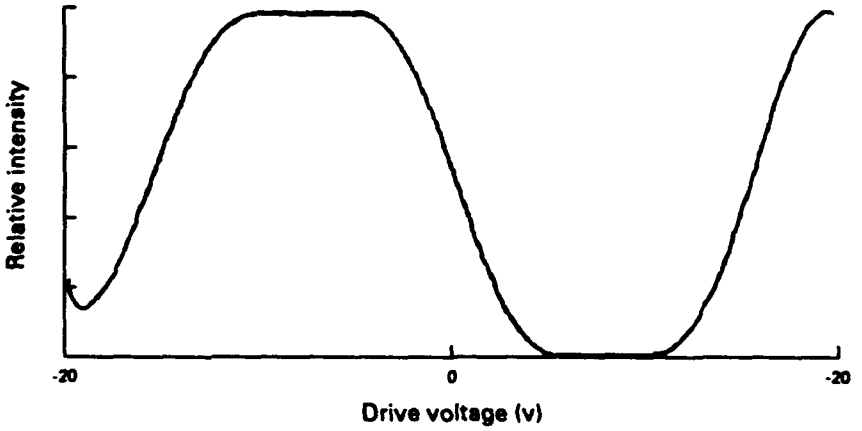

Figure 3-8. Measured Transfer Characteristic for a Two-Conductor Digital Switch

The linear scale of figure 3-8 does not allow an accurate representation of the crosstalk properties of the digital switch. Data for a different device of this family is plotted logarithmically in figure 3-9. This result shows crosstalk suppression at or below -20 dB over about 50% of the switching range. This is about a five times larger range than for a conventional Mach-Zehnder balanced bridge switch. Crosstalk at the -20-dB level is satisfactory for enabling operation of the HOE-ADC at precision up to about 6 bits.

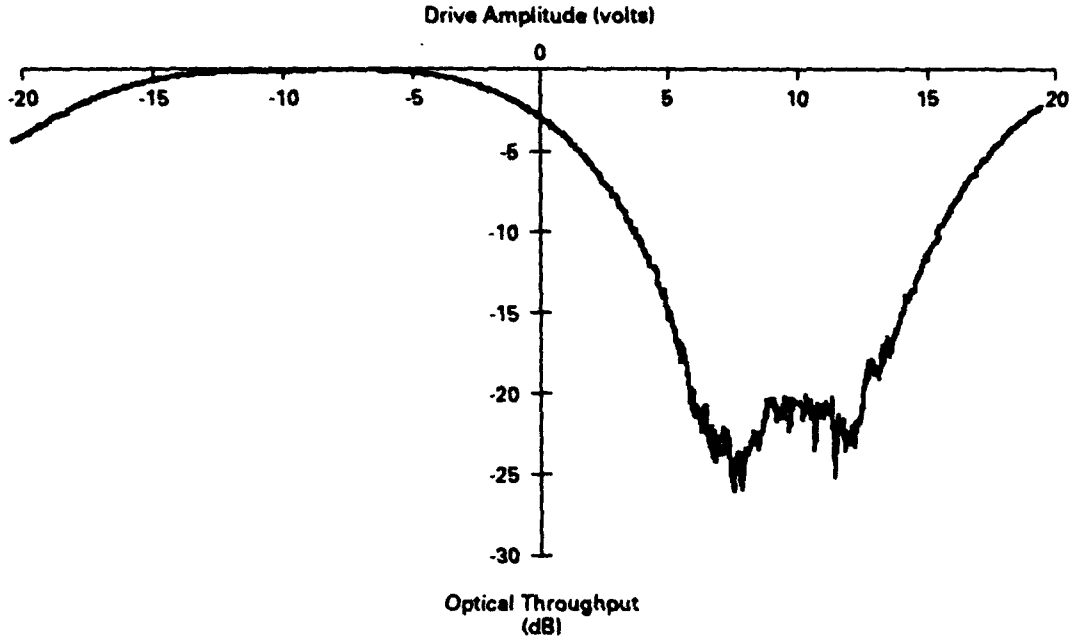

Figure 3-9. Crosstalk Measurement for Two-Conductor Digital Switch

For optimum high-frequency performance, it is desirable to minimize electrode resistance by using relatively thick electrodes (greater than 2,000 nm). This was first tried by electroplating a thick gold layer onto a patterned base. We had used this process very successfully for wideband Mach-Zehnder modulators having bandwidths beyond 30 GHz. However, in the digital switch, we found that the digital transfer characteristic was significantly degraded. We believe this was due to an alteration of the coupling constant due to stresses induced by the electroplating process.

We then pursued E-beam deposition, in conjunction with a liftoff process, as an alternative for producing thick electrodes. The thicker photoresist layers required a different formulation of photoresist from what we had previously used. Aggravated by the small feature size of the digital switch, adhesion problems were encountered between this new resist and the SiO_2 buffer layer. To counter this problem, we used an adhesion promoter that had not been previously used. With this adjustment, we did achieve the desired thickness of electrodes with the E-beam process. Measurement of the DC switching voltage showed no change for the thick electrodes, as expected. However, it was observed that DC drift in the device was essentially eliminated. This is not necessarily desirable for the digital switch on z-cut $LiNbO_3$ because it prevents the redistribution of pyroelectrically generated charge. Inhibition of this redistribution can adversely affect the digital characteristic by introducing a temperature dependence. In other words, the digital switch characteristic could degrade if a high drive power level was required with an accompanying elevated temperature. This turned out to be the case, as will become evident later in this section.

We then proceeded to evaluate the frequency response of the two-conductor digital switch. Typical values measured for the low-frequency capacitance and the resistance of the electrodes were 12 pf and 5Ω respectively. The calculated frequency response, driven from a 50Ω source, is shown as the solid curve in figure 3-10. The calculated response with an 8-nh shunt inductance is represented by the dashed line. This simple matching circuit should thus reduce in the drive power by about 4 dB at 500 MHz. To reach higher frequencies would require more advanced matching strategies, such as transformer matching, to achieve peak response over a narrow band. The rigors of the experimental exploration of the design and fabrication parameters for the digital switch, along with funding and scheduling constraints, did not permit advancing to more optimum matching techniques during this program. We did proceed to demonstrate the digital switching characteristic at frequencies up to near 500 MHz, as discussed next.

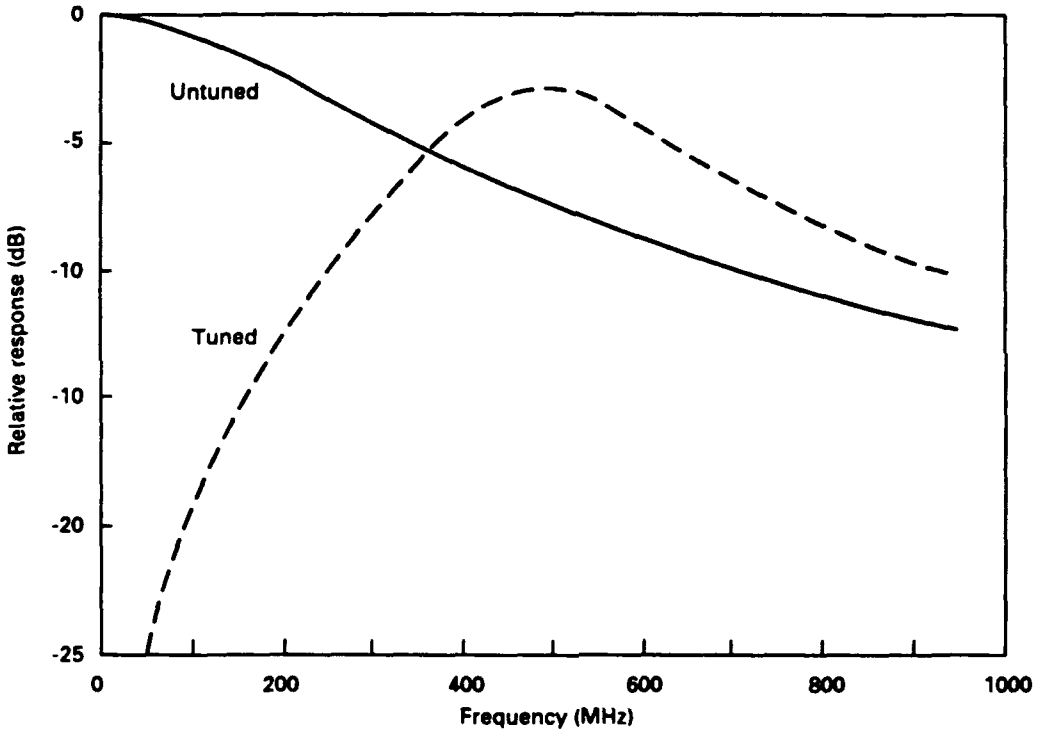

Figure 3-10. Calculated Frequency Response for a Lumped-Element, Two-Conductor Digital Switch. The solid line is for no matching. The dashed line is for an 8 nh shunt inductance.

The high-frequency testing was done on devices that were part of a 1x4 switch array in the layout shown in figure 3-11. The overall length of the substrate was 55 mm; the overall active electrode length for each switch was 15 mm; the interwaveguide gaps in the switching regions were 13.8 μm. At the output side of the substrate, the channels fanned out to spacings of 150 μm to enable coupling to optical fibers mounted in a silicon V-groove fixture. To facilitate testing and use in the A/D converter, the switch array was packaged with RF connectors and fiber-optic pigtails. The average optical insertion loss of the channels was about 5 dB. This was about 6 dB better than the commercial switch array previously used and met our objectives for this task.

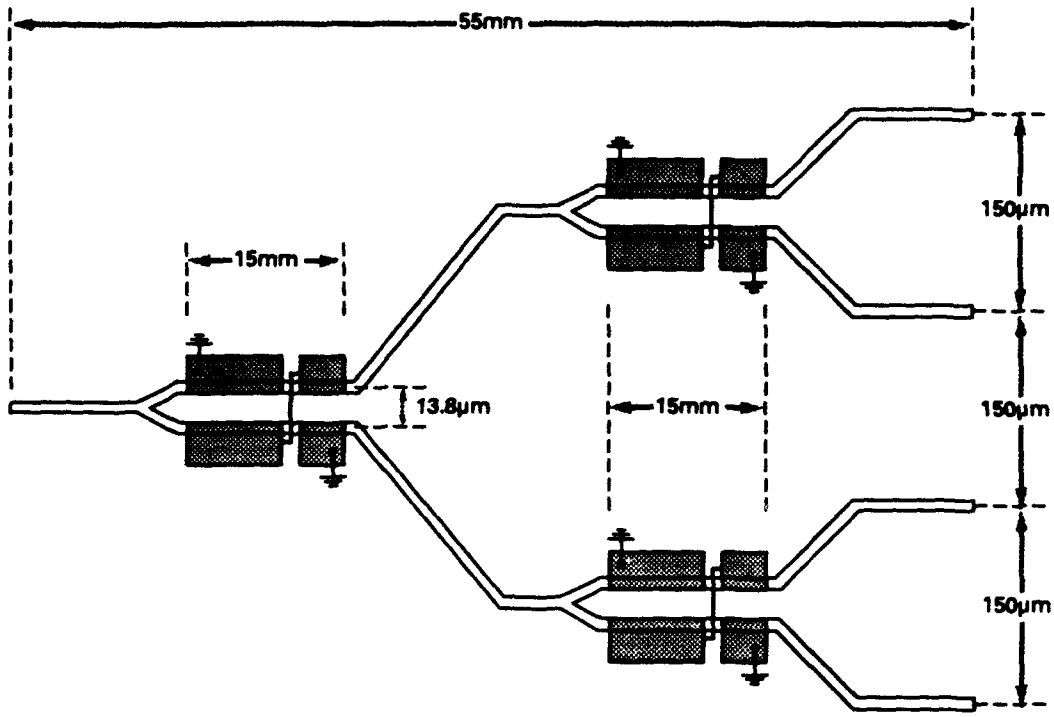

Figure 3-11. Layout of the 1x4 Digital Switch Tree

The frequency response for one of the unmatched switches is shown in figure 3-12. The overall rolloff is as predicted in figure 3-10 except for the severe dip near 1 GHz. That feature is attributed to destructive interference at that frequency from reflections at the ends of the electrodes. This was corroborated by the addition of a ribbon wire to extend the electrode length. The effect was to shift the dip to a lower frequency, as expected. When a shunt inductance of 8 nh was added to the switch (see figure 3-13), the frequency response became peaked near 500 MHz, in good agreement with the prediction of figure 3-9.

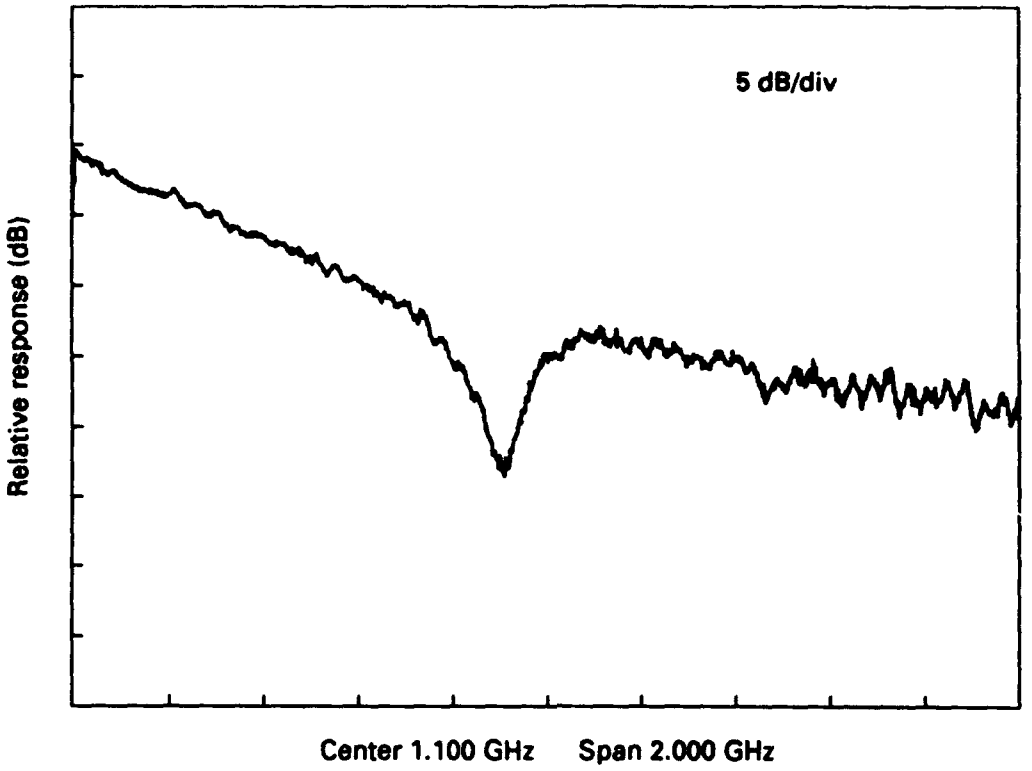

Figure 3-12. Frequency Response of an Unmatched Two-Conductor Digital Switch

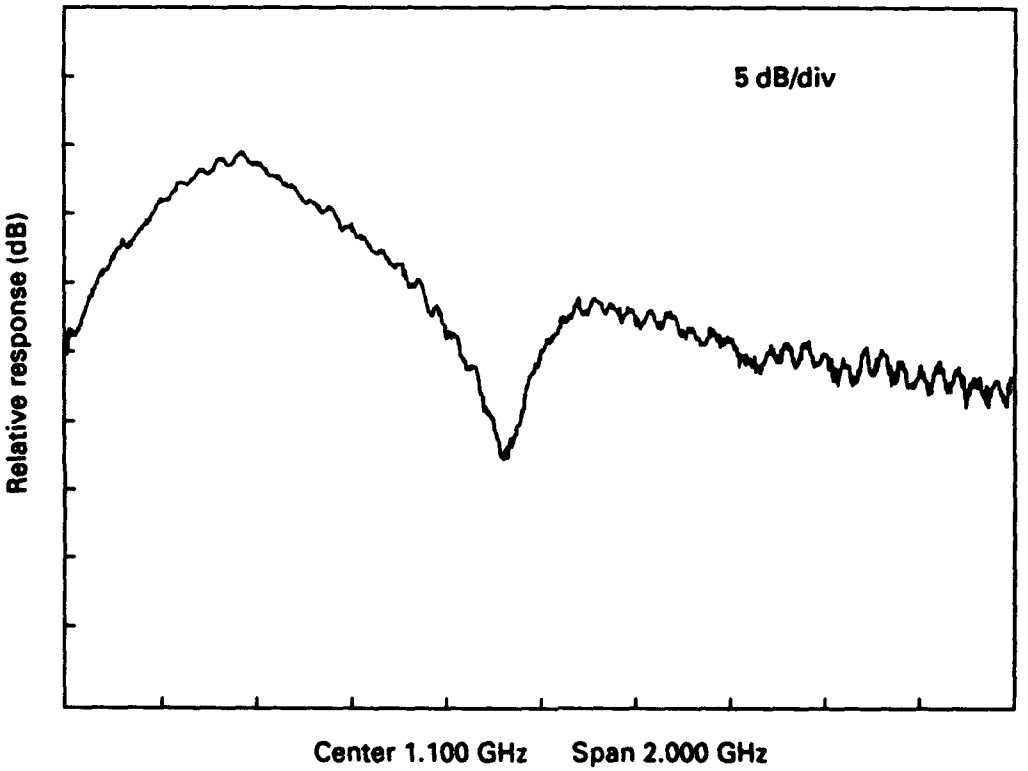

Figure 3-13. Frequency Response of a Two-Conductor Digital Switch With an 8-nh Shunt Inductor

Figures 3-14 and 3-15 show typical time-domain response of the digital switches at 100 and 200 MHz respectively at a drive level of 500 mW with no matching. In the former case, the device is clearly exhibiting the expected flat output regions in the off and on states. However, in the latter case, the drive level is apparently not high enough to reach the fully switched voltage regime. At 500 MHz (not shown), switching was very incomplete. To enhance the 500-MHz performance, a shunt inductance was added to improve the electrical matching. The time-domain response of figure 3-16 was recorded. Aside from a small bias, the figure shows the switch operating essentially in a fully switched regime. Close inspection of the fully-on region of the trace reveals a slight dip, suggesting the digital characteristic is deteriorating. Operation at higher power levels showed an even greater degradation. We believe this is a result of the loss of electrical conductivity in the oxide buffer layer, discussed previously. At high drive levels, resistive heating in the electrodes caused local heating of the switch. The result is unrelieved piezoelectrically induced stress that alters the coupling constant of the directional coupler, resulting in deterioration of the digital characteristic. If it were not for this effect, the fabricated switch array could have been driven harder and operated at frequencies useful in the A/D converter demonstration.

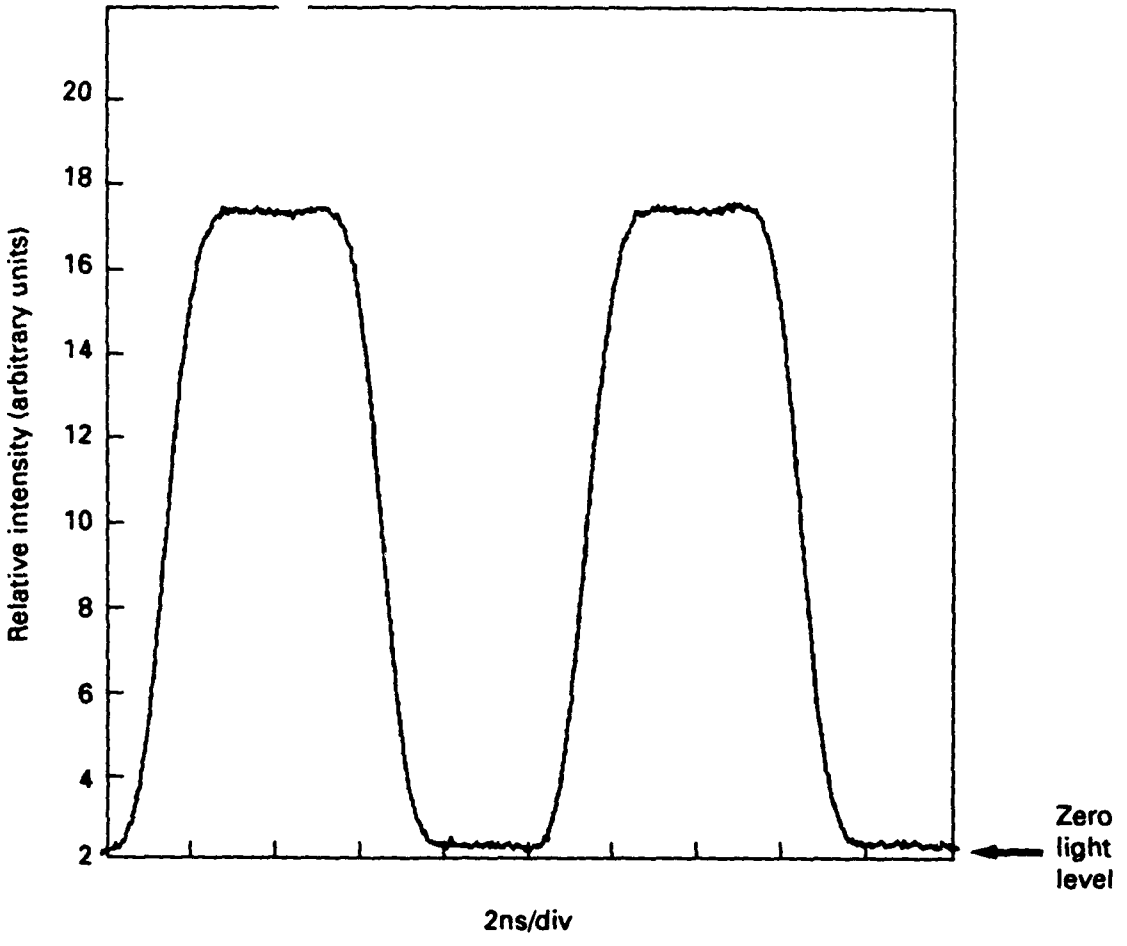

Figure 3-14. Time-Domain Response of the Digital Switch at 100 MHz (Unmatched)

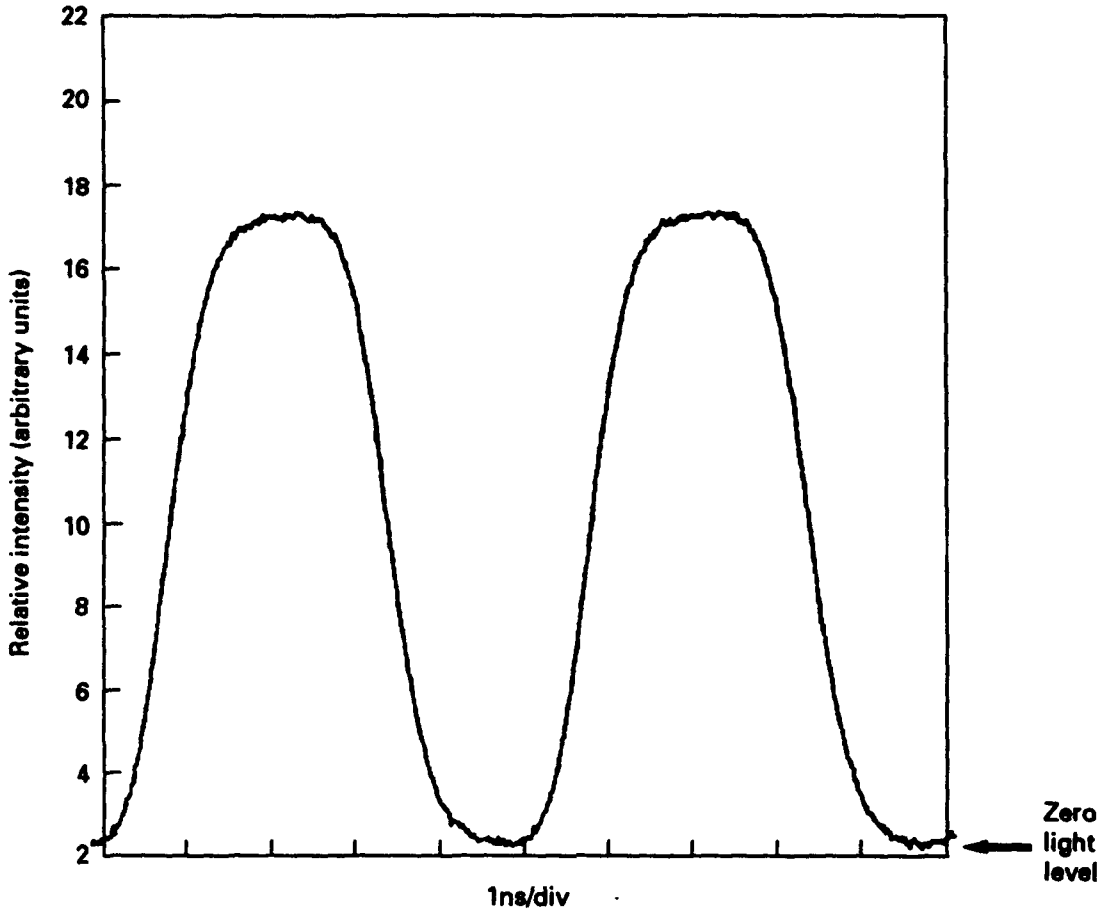

Figure 3-15. Time-Domain Response of the Digital Switch at 200 MHz (Unmatched)

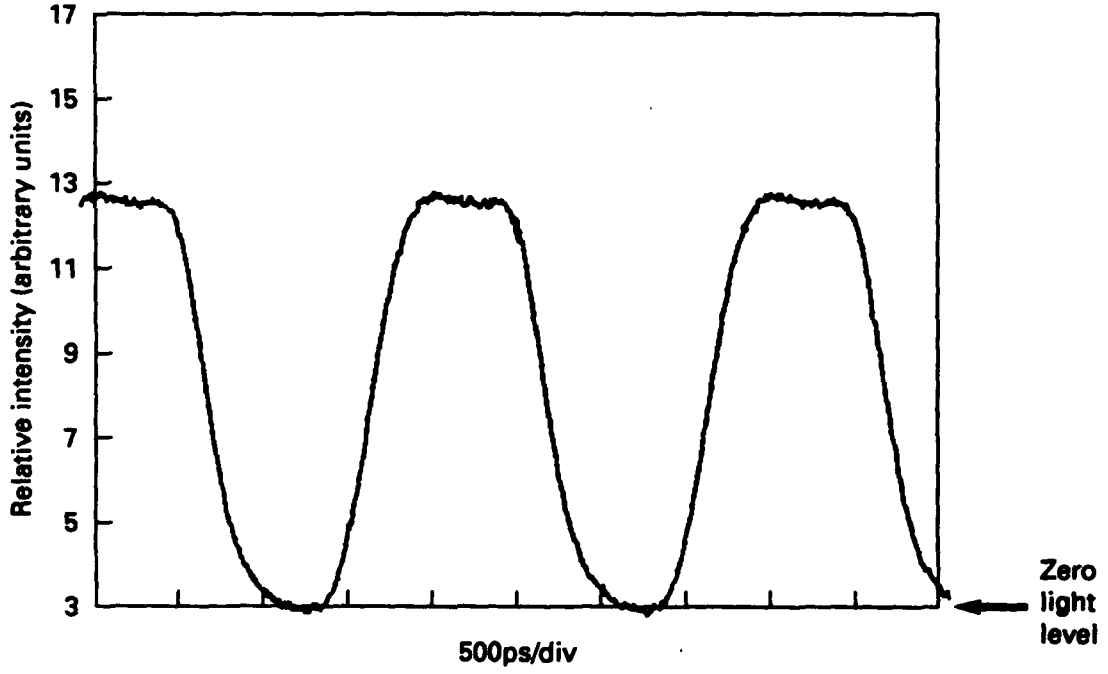

Figure 3-16. Time-Domain Response of the Digital Switch at 500 MHz (Matched With 8-nh Inductor)

In conventional directional-coupler switches with delta-ß reversal electrodes, independently addressed electrodes allow fine tuning for crosstalk suppression. In the digital switch, both electrode sections have the same applied voltage. This removes a degree of freedom in voltage control and puts the burden on fabrication tolerance. Directional-coupler optical waveguide devices, including this digital switch, are particularly sensitive to variations in fabrication. As design rules are not well established for the fabrication of this type of device, fine tuning the design of the digital switch involves experimental determination of the key parameters based on evaluation of sets of devices with a systematic variation of the key design parameters. This is a time-consuming, labor-intensive activity. The digital switch also imposes processing constraints not found in other switches. For example, it is particularly sensitive to fabrication-induced strain. This problem was encountered when electroplated electrodes were attempted. Time and funding limitations did not permit design of a third-generation device with more advanced matching and optimized electrical conductivity in the buffer layer. This would have allowed operation at the 2-GHz speed needed for the advanced HOE-ADC demonstration. In spite of this, successful simulation testing of the A/D converter at advanced performance levels was possible using a wideband modulator made at Boeing as a 1 GHz on-off switch. This is discussed in section 4.0.

4.0 4 GS/s SINGLE-CHANNEL HOE-ADC SIMULATION

The final phase of this contract consisted of laboratory tests that simulated a single channel of a four-channel HOE-ADC with a 4 GS/s sample rate. From the work we performed previously with our fully implemented four-channel system, we learned that operating multiple channels in parallel was straightforward and that system performance was largely determined by the performance of an individual channel. A block diagram of the single-channel system we assembled is shown in figure 4-1. As we had shifted to a 1,530-nm laser source to be compatible with the fiber amplifier, we were unable to make use of the guided-wave components used in the previous system that used a 1,300-nm source. The modulator we used was fabricated within Boeing and has substantially better efficiency and lower insertion loss compared with the previously used component. We planned initially to operate the pulsed laser at 4 GHz and to drive a 1x4 optical switch array as we had previously. However, the only optical switch available to us that could operate at 1 to 2 GHz with 1,530-nm light was a 1x2 device. We decided to reduce the laser pulse rate to the cavity fundamental at 2 GHz and drive this single switch at 1 GHz. Thus, the sample rate from the single output we tested was 1 GHz, exactly as it would be in a four-channel, 4 GHz system. We sent the resulting pulse train to the same Lasertron receiver we had used previously. After subsequent amplification, we digitized these pulses with the use of a Tektronix model DSA-602 oscilloscope. The record length for data we acquired using this instrument was set to 8,192 samples. Like the HP-54111D described earlier, this instrument used an internal sampling clock to which we approximately synchronized the generator driving the laser and switch.

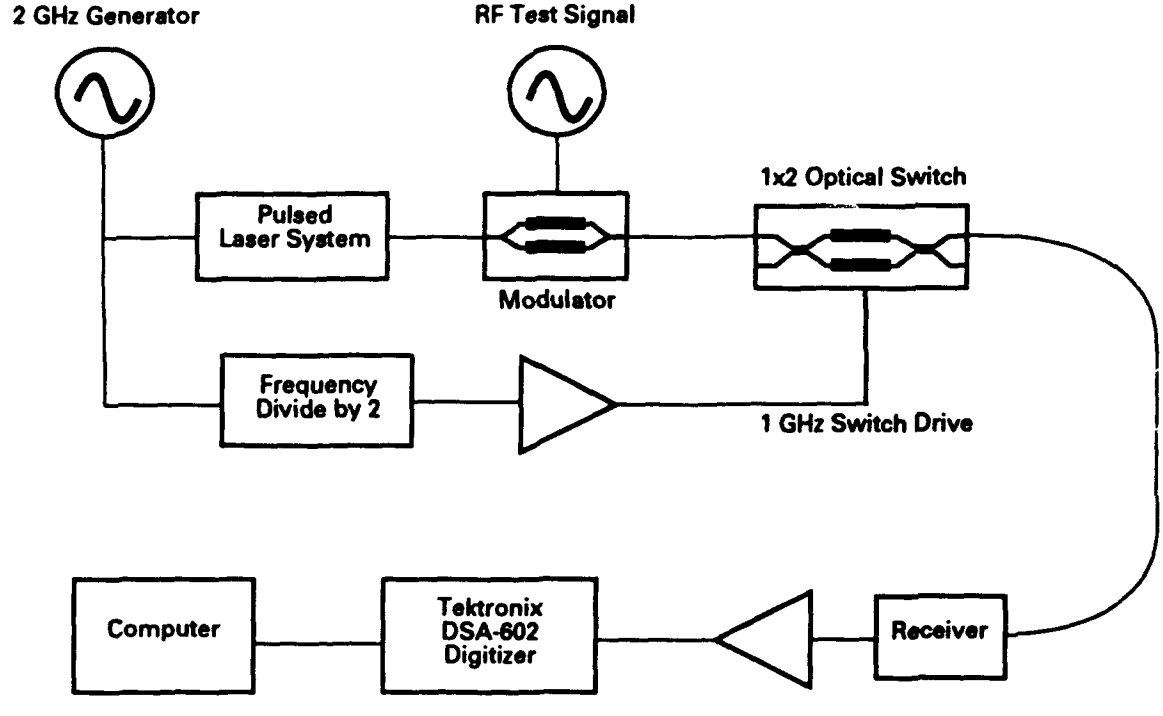

Figure 4-1. Schematic of Single-Channel HOE-ADC Simulation

The characteristics of the 1,530-nm modelocked laser used in these tests were discussed in section 2.2. With the exception of an increased threshold current, we confirmed that the laser behavior had not changed significantly since the time of these earlier tests. The average optical power at the input to the fiber amplifier was 57 μW, and with maximum bias current to the pump laser in the amplifier, the power output from the amplifier was 7.6 mW. Most of this power is unfortunately due to spontaneous emission within the fiber amplifier, and following the narrowband filter that suppresses this background light, we are left with 3.0 mW.

We used a $LiNbO_3$ traveling-wave modulator that was designed and fabricated within the optical guided-wave group at Boeing for a separate application. It was packaged in an RF mount, but fiber pigtails had not been attached. At the input to the modulator we butt-coupled a single-mode fiber that had an FC/PC connector attached to the opposite end. We used the same electrical drive circuit that was used earlier for the four-channel system. We found that the switching voltages at our two main test frequencies of 10.125 GHz and 125 MHz were 18V and 8.3V respectively.

The optical switch was also designed and fabricated within the optical guided-wave group at Boeing. It was a bare $LiNbO_3$ chip that was not mounted in an RF package. A polarization-preserving fiber was axially aligned and butt coupled to both the output of the modulator and the input to the switch. The RF input to the switch was attached to a Cascade probe mounted to contact lumped-element electrodes. The electrical drive was a 1-GHz, 28-dBm sine wave produced by the same frequency divider circuit used in the four-channel system. While monitoring the channel crosstalk of the received pulses on a sampling oscilloscope, the phase and amplitude of this drive signal were optimized. Also, the polarization of the light input to the modulator was adjusted for an optimal extinction ratio by using a half-wave plate and a fiber-polarization controller, (ordinarily a fiber-polarization controller would suffice, but ours was intended to operate with 1,300-nm light). We achieved a DC extinction ratio of 16 dB with this switch though it would have certainly been improved if we had used optimal polarization components. The resulting channel crosstalk arising from incomplete switching is only slightly evident in the results from the sampling oscilloscope shown in figure 4-2. In the lower trace, the switch was being driven, and alternate pulses from the laser are switched off to produce the 1-GHz pulse train from the single output channel. In figure 4-3 another trace from the sampling oscilloscope is shown in which the modulator was driven at 10.2 GHz and the switch was operating. This trace shows the effect of sampling in the bandpass mode since the *apparent* frequency of the sampled sine wave is 200 MHz.

Between the output of the blocking filter and the receiver, the optical insertion loss was 9.5 dB. This is substantially improved from the earlier four-channel system in which the insertion loss between the laser and receivers varied among the four channels between 14.8 and 18.6 dB. The average power to the receiver when the entire single channel test system was operating and the fiber amplifier was at maximum gain was 110 μW and exceeded the saturation level for the receiver. To work within the dynamic range of the receiver, we had to reduce the fiber amplifier gain by 3 dB. Consequently, if a 1x4 switch array were used in this system, similar performance would be expected upon returning the amplifier to the maximum gain level.

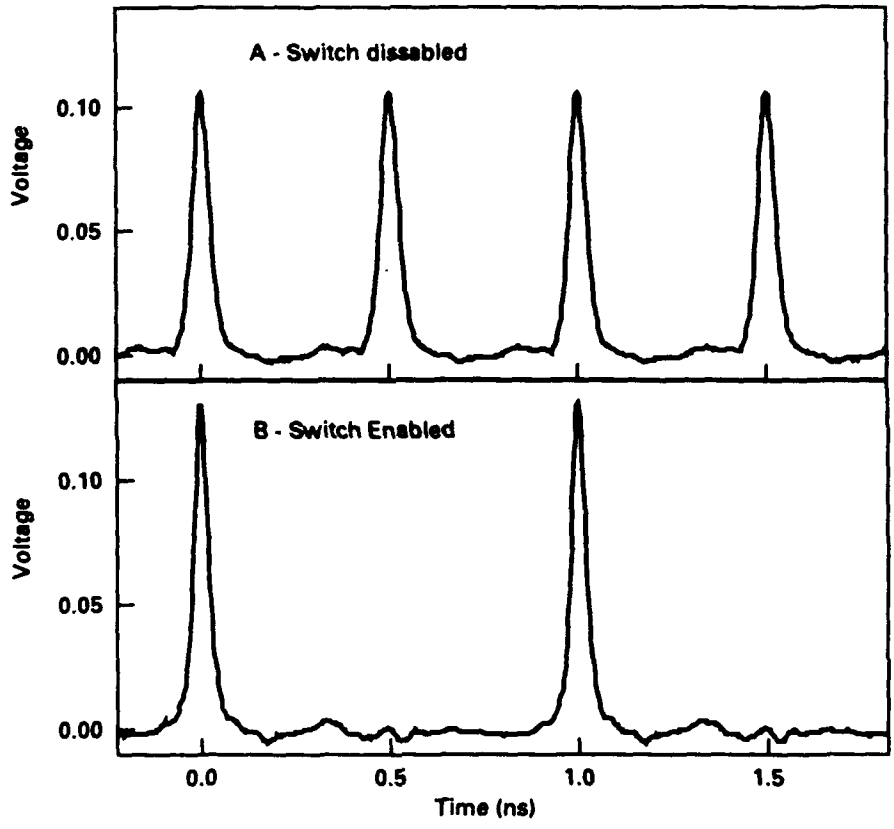

Figure 4-2. Detected Laser Pulses After Switch: (a) Switch Disabled, (b) Switch Running

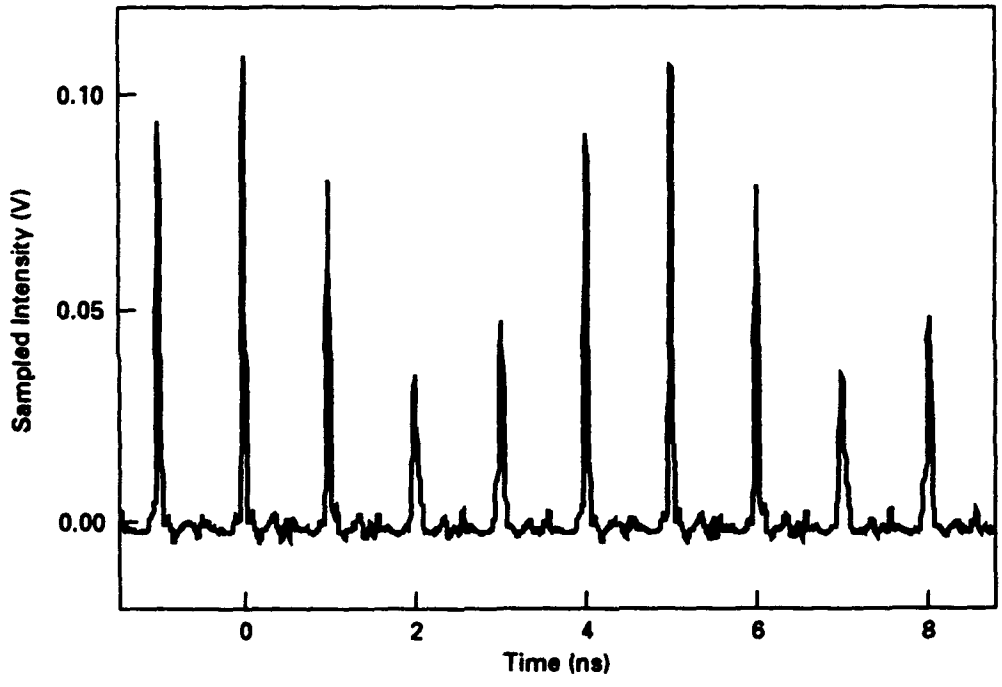

Figure 4-3. Detected Laser Pulses With Modulator Driven at 10.2 GHz

In summary, the most significant differences between this test system and the four-channel system described earlier are (1) the pulsed-laser stability is improved; (2) an optical amplifier is installed; (3) the optical insertion loss is improved; and (4) the digitization rate of an output channel is doubled. The remainder of this section discusses the results of tests conducted with this system. These tests closely matched those carried out previously by using the four-channel system. An exception is that we did not carry out measurements of the frequency response across some selected band, but instead made isolated measurements at only a few frequencies. This was a practical limitation imposed by the lack of long-term synchronization between the pulsed laser and the Tektronix digitizer we used.

4.1 Bandpass-Mode Testing

Because the electronic hardware from the four-channel system was available, we picked a nominal operating band of 10 to 12 GHz. For a fully implemented four-channel, 4-GHz HOE-ADC system, this choice of bands would lead to the sampled frequency distribution being translated *and reversed* (as shown in figure 2-2). Whether this effect would be acceptable is application dependent. For the purposes of the single-frequency testing we conducted, this artifact is of no importance.

Shown in figure 4-4 is a small portion of a data record obtained from the system when driven by a 24-dBm, 10.125-GHz signal. The modulation index in this case was m=0.77. In the 1-ns time span between samples, the signal has gone through 10.125 periods. Using the entire 8-μs record, the power spectral density of this acquisition was calculated and is shown in figure 4-5. The only significant spurs in the spectrum are a consequence of second- and third-order distortion. The noise level in this power spectrum was found to be slightly elevated in regions shifted by roughly 11 and 32 MHz to either side of both the signal frequency and DC (which is mapped to 10 GHz in this figure). These noise bands were also seen adjacent to the harmonics of the laser pulse rate from measurements of the RF spectrum of the detected laser pulses. Following a sine wave fit to this dataset, we determined the precision to be 3.8 effective bits.

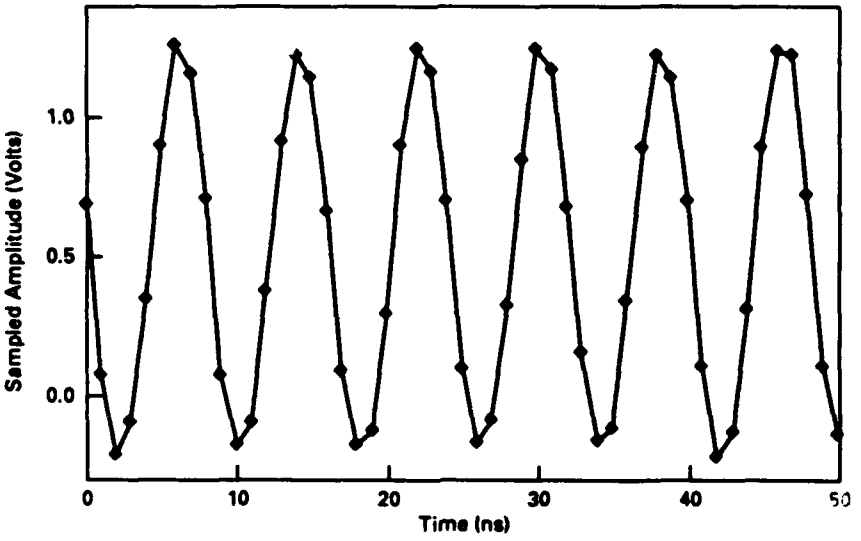

Figure 4-4. Sampled Data Obtained From One-Channel System, f = 10.125 GHz

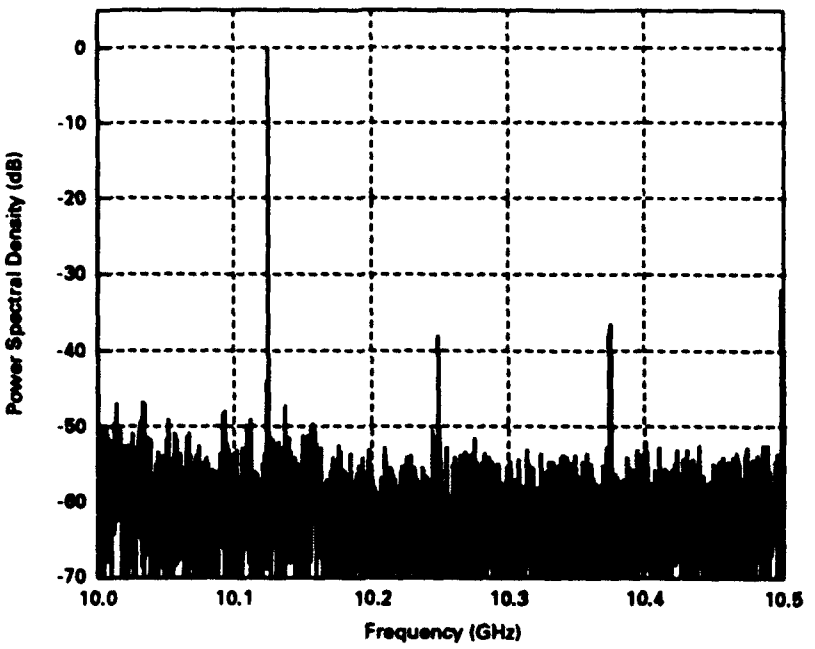

Figure 4-5. Power Spectrum Calculated From a Single Data Record, f = 10.125 GHz

4.1.1 Phase Dependence of Noise

Using the data record shown partially in figure 4-4, we carried out an analysis of the phase dependence of the noise. We expected to follow the same procedure discussed in Section 2.4.1, which allowed us to quantify the noise introduced by laser pulse jitter. Following the same procedure described previously, we first plot the sampled data versus the signal phase as shown in figure 4-6. Figure 4-7 shows residuals of the samples to the sine-wave fit versus phase; using these residuals, we calculated the relative power phase density. These values of the relative PPD were averaged over 10-deg phase spans and are plotted in figure 4-8.

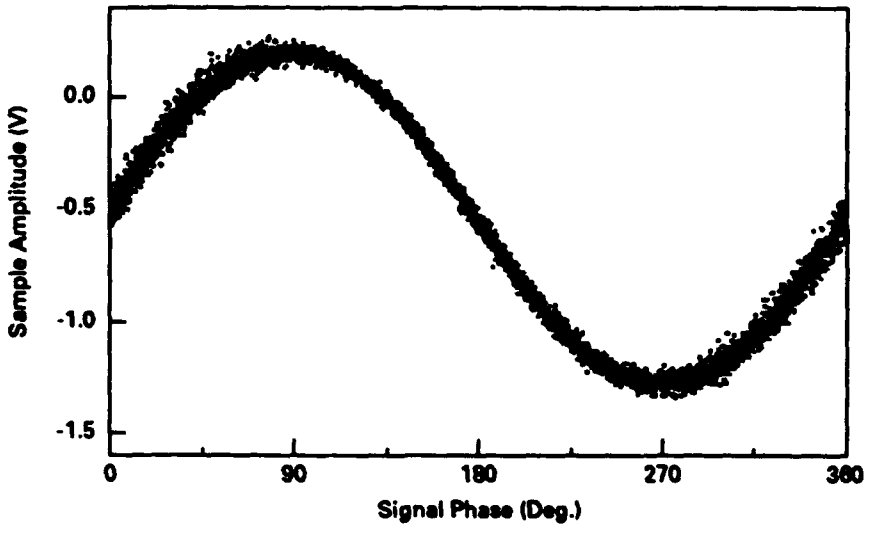

Figure 4-6. Sampled Data Versus Signal Phase; f = 10.125 GHz

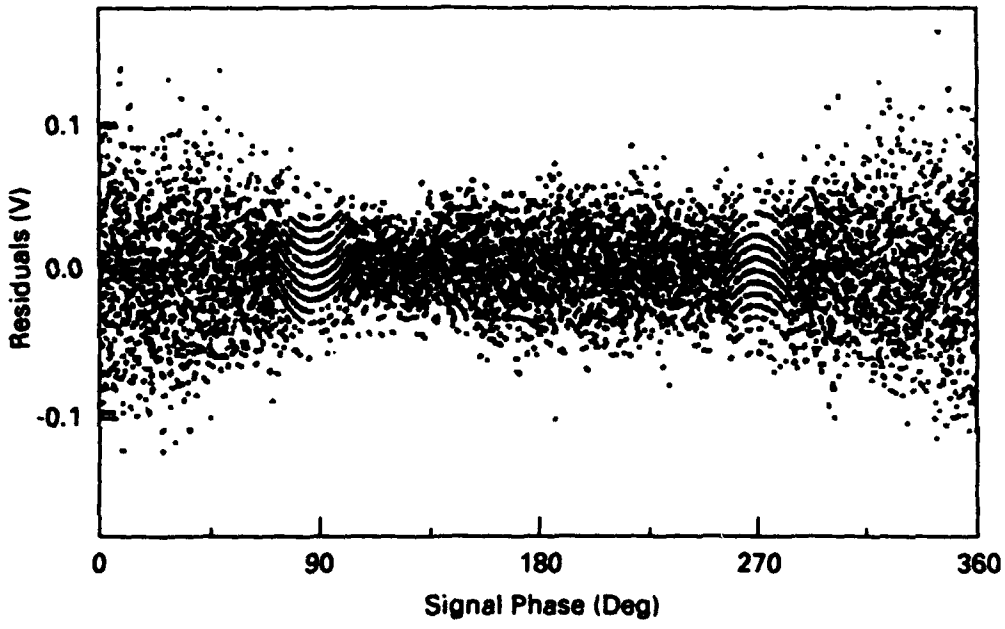

Figure 4-7. Residuals to Sine-Wave Fit Versus Signal Phase, f = 10.125 GHz

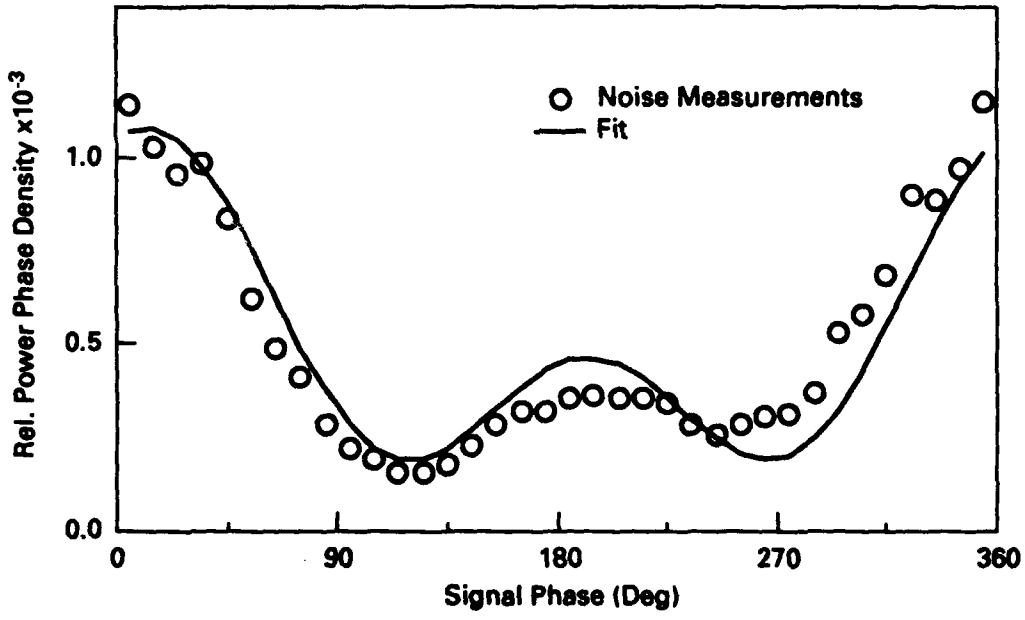

Figure 4-8. Relative Power Phase Density and Fit to Modeled Laser Noise, f = 10.125 GHz

At this point we were surprised to find a significant departure from the result we had seen previously. The noise peak at a phase of 180 deg was now much smaller than the peak at 0 deg. A superposition of the separate PPDs for laser RIN and jitter from equations 2-14 and 2-18 fails to resemble the data displayed in figure 4-8. A possible explanation for this result is that fluctuations of the laser pulse energy and timing are not statistically independent as we have previously assumed. For example, imagine that a particular pulse that is slightly delayed from its intended time also contains slightly

more energy than the average pulse. If this pulse passes through the modulator while its transmission is decreasing, then these coincident fluctuations would produce errors that partially compensate for each other. If instead the modulator transmission is increasing when the pulse passes through, the two errors would add constructively.

An empircal model of such correlated fluctuations can be described by a linear relation between fluctuations of pulse energy and pulse timing:

$$\delta\tau = \alpha \frac{\delta E_p}{E_p} \tag{4-1}$$

where α is a constant and E_p is the average pulse energy. Similar to equation 2-16, the error in a sample voltage that results from simultaneous errors in pulse timing and energy is given by:

$$\begin{aligned} \delta S_{RIN/JITTER} &= gE_p \left\langle \left(1 + \frac{\delta E_p}{E_p}\right) T(t+\delta\tau) - T(t) \right\rangle \\ &\cong \frac{gE_p}{2} \left\langle 2m\cos\theta \sin\left(\frac{\omega\delta\tau}{2}\right) + \frac{\delta E_p}{E_p}(1 + m\sin\theta) \right\rangle \end{aligned} \tag{4-2}$$

where T(t) is the modulator transmission from equation 2-1 and $\theta = \omega t$. Combining equations 4-1 and 4-2 we obtain:

$$\delta S_{RIN/JITTER} \cong mgE_p\delta\tau \left\langle \frac{\omega}{2}\cos\theta + \frac{1}{2\alpha}\left(\frac{1}{m} + \sin\theta\right) \right\rangle \tag{4-3}$$

f $\delta\tau$ is now treated as the variance for a normal distribution of pulse timing fluctuations, the relative power phase density is given by:

$$\begin{aligned} PPD_{RIN/JITTER} &= \frac{\left\langle \delta S^2_{RIN/JITTER} \right\rangle}{2\pi \left\langle S^2_{AC} \right\rangle} \\ &= \frac{4\delta\tau^2}{\pi}\left[\frac{\omega}{2}\cos\theta + \frac{1}{2\alpha}\left(\frac{1}{m} + \sin\theta\right)\right]^2 \end{aligned} \tag{4-4}$$

Using this new expression for the power phase density, a fit to the data shown in figure 4-8 was performed in which $\delta\tau$, α, and a constant offset were free parameters. The solid line plotted with the data is the resulting fit, and it is in good agreement with the measurements. The parameters obtained from the fit are $\delta\tau$ = 0.63 ps, α = 70 ps, and constant offset = 1.9 x 10^{-4} radian^{-1}. From equation 4-1 the variance of the energy fluctuations is predicted to be 0.9%. The laser pulse jitter estimated by applying this model is somewhat less than the estimate of 1.4 ps obtained from measurements of the RF spectrum of the detected laser pulses. However, in the spectral analysis

method, it is also an assumption that phase and amplitude noise terms are uncorrelated. Hence, those results could be in error if these fluctuations are indeed dependent.

4.1.2 Dependence of Precision on Optical Power

From the noise analysis in section 2.3, some of the noise sources are dependent on the optical power level at the receiver and others are invariant. Estimates for the laser noise arising from both jitter and pulse energy fluctuations were obtained from the data analysis in the previous section. Much of the remaining noise is expected to originate within the receiver electronics. To test this hypothesis, we measured the precision of the system over a range of optical power levels. The optical power level at the receiver, was varied by inserting calibrated optical attenuators before the receiver and separately by reducing the gain in the EDFA. It is important to note that the optical power level was varied while all the other parameters held constant. Some of the reduction in SNR resulting from a reduced optical power is recoverable by increasing the amplifier gain following the receiver. However, this would greatly complicate interpretation of the results. Measurements from both of these methods are plotted in figure 4-9. One immediate conclusion obtained from these two datasets is that varying the optical power by either method leads to similar results, and hence, there is no significant excess noise contribution from the EDFA. However, we did not attempt to rigorously characterize the noise introduced by the EDFA, and some associated degradation may become significant if the other noise sources are much reduced.

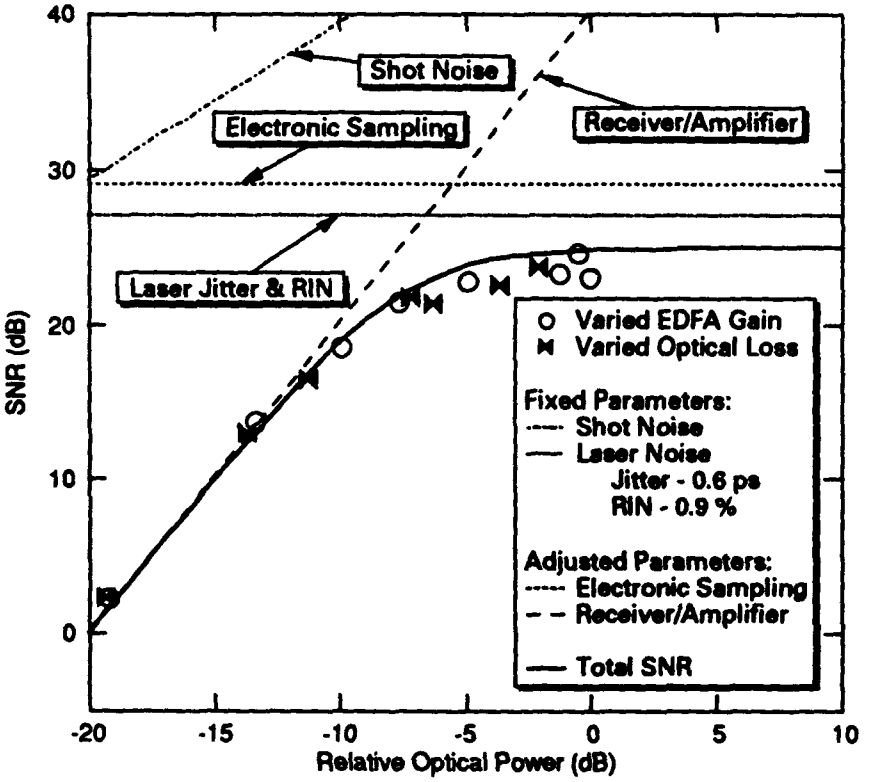

Figure 4-9. Measured SNR Versus Optical Power Together With Estimated Noise Sources

The contributions to the system SNR from laser jitter, pulse energy fluctuations, and shot noise are shown as dashed curves in figure 4-9. These noise terms are based on the measured optical power in the case of shot noise and the results of the previous section in the case of laser noise. Another dashed curve is shown that accounts for receiver noise that depends on the optical power level as derived in equation 2-20. The magnitude of this term was adjusted in order to agree with the measured precision at low optical power levels. With this single free parameter, it was not possible to obtain good agreement between the combined system precision and the measured precision at high optical power levels. This led to the conjecture of another significant noise source arising from *electronic* sampling noise. The idea of this error source relates to the signal arriving at the electronic sampling circuitry consisting of a series of pulses—one for each sample. Such a signal is quite different from signals typically sent to A/D converters because the power spectral density has significant content at the sampling frequency and above. Slight timing fluctuations on the sampling points of this pulsed waveform would lead to errors in much the same way that jitter of the laser pulses leads to errors in the *optical* sampling process. Because the magnitude of errors arising by such a process would be proportional to the signal, the resulting degradation to the SNR would not depend on optical power level. A final dashed curve in figure 4-9 accounts for this noise source and the level served as a second free parameter in fitting the combined system noise to the measured precision. This resulting fit is the solid curve in figure 4-9. To the extent that this modeled system noise represents the real system, it is clear that any further gain in optical power would not yield improved precision unless the laser noise, and perhaps the conjectured electronic sampling noise, are much reduced. As a practical point, to avoid saturation of the present receiver, the optical power level could not exceed roughly 50% of the maximum power available at full gain from the EDFA.

4.2 Baseband-Mode Testing

The single-channel system was also characterized at baseband using a sine-wave drive at 125 MHz. By sampling such a low-frequency signal, it is possible to test the interpretation of the noise from the previous section. We expect the importance of laser pulse jitter to become insignificant at this low frequency, as was the case in section 2.4 for the four-channel system. Therefore, the power phase density is predicted to qualitatively resemble the previous baseband results shown in figure 2-11. Following the same analysis used in section 4.1 with data collected from the 125-MHz signal, the PPD was determined and is plotted in figure 4-10. Also shown on this plot is a solid curve that represents the *predicted* PPD based on the same parameters used in fitting the data in figure 4-8. In other words, there were no free parameters for the solid line in figure 4-10, and the only change from the analytical curve shown in figure 4-8 results from the reduction in signal frequency. By the good agreement between the measured and predicted PPD results for this 125-MHz case, our interpretation of the various noise sources seems well justified.

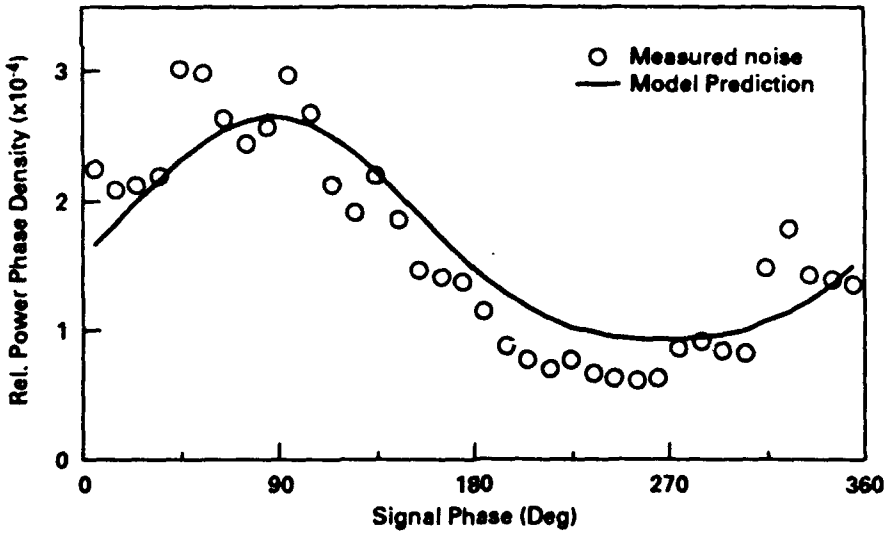

Figure 4-10. Relative Power Phase Density and Fit to Modeled Laser Noise, f = 125 MHz

The best precision obtained at 125 MHz was 4.6 effective bits, which represents the best precision yet demonstrated by an optical A/D converter. The power spectrum of this data is shown in figure 4-11. The most conspicuous noise bands are peaked at 13 and 32 MHz and coincide with noise bands observed independently while characterizing the pulsed laser. A final test was to determine the system performance when the laser amplifier is bypassed. In this case, the optical power arriving at the receiver was reduced to 2 μW, and the optimized precision was 3.2 effective bits.

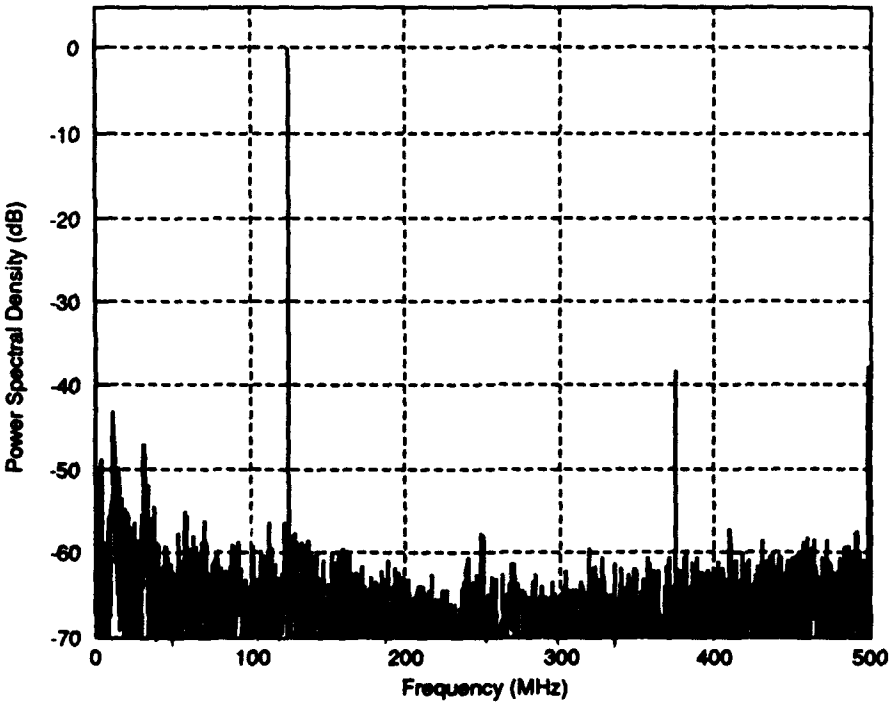

Figure 4-11. Power Spectrum Calculated From a Single Data Record, f = 125 MHz

In conclusion, the system operation in bandpass mode was primarily limited in precision by the laser pulse jitter. Determination of the jitter by analysis of the phase power density led to our conjecture of correlation between jitter and pulse energy fluctuations. This point is significant because the spectral noise analysis often applied to pulsed laser characterization assumes these noise sources are independent. The best precision obtained in the passband mode was 3.8 effective bits, and in the baseband mode, 4.6 effective bits. For operation at baseband, the precision is limited about equally by laser RIN and receiver noise. Owing to the low power obtained from our pulsed semiconductor laser, the precision is substantially improved by the incorporation of an Erbium fiber amplifier.

5.0 SUMMARY

5.1 Recommendations

Presently, there are digitizing circuits available from both Tektronix and Hewlett-Packard with a sampling rate of 1 and 2 GHz respectively. The card from Tektronix has a bandwidth of ≈1 GHz and makes use of two interleaved A/D converters that each sample at 500 MHz. The Hewlett-Packard card has a bandwidth of 1.5 GHz and also uses two interleaved A/D converters. Both of these components use bipolar silicon technology. Following discussions with people at HP, it seems reasonable to expect a two to four-fold increase in both sampling rate and bandwidth in the next several years. For the HOE-ADC approach to offer a continued advantage, it must be capable of making use of such future developments; for example, a laser pulse rate of 16 GHz, 1x4 demultiplexing, and 4-GHz electronic A/D converters.

A conclusion from our test results is that our principal performance limitation was due to noise originating within the pulsed laser source. It is clear that any future work in this area that seeks to improve upon the precision we have demonstrated must develop a highly stable pulsed laser. We can suggest two alternatives to the mode-locked semiconductor laser that would be worthy of further research.

The first of these approaches relies on intensity modulators that are external to a stable continuous wave laser. This has the advantage of separating the requirements on average power and intensity stability from the pulse characteristics. The complicated and sensitive dynamics of a pulsed laser can thus be exchanged for the simple and well-behaved dependence of transmission on applied voltage that exists for electro-optical intensity modulators. However, an inherent disadvantage is that the peak intensity is limited to the average intensity from the continuous-wave (CW) laser, and for low duty-cycle pulses most of the light is wasted. By using a diode-pumped solid-state laser, this power penalty may not be a significant limitation. For example, commercially produced, single-frequency Nd:YAG lasers are available with CW output power as high as 300 mW and with relative intensity noise (RIN) less than -160 dB/Hz. An appealing design for the external modulator consists of two Mach-Zehnder intensity modulators in series each driven by a sinusoidal drive voltage at the frequency of the desired pulse rate. One of the modulators would be biased to a transmission maximum so that a pulse would be transmitted during each zero crossing of the sine-wave drive. The second modulator would act as a switch that blocks alternate pulses to eliminate the systematic jitter that would be introduced by errors in the bias point of the first modulator. This arrangement is a modification upon a set of modulators described previously that was susceptible to this form of jitter. This new combination yields well-formed pulses having a width of 17% of the sample period. Such pulses would be too broad to perform well in the bandpass mode, but, they would be acceptable for baseband operation. Since the modulators only need to respond to a single-frequency drive voltage, pulse rates as high as 20 GHz are certainly attainable.

The second approach consists of a mode-locked solid-state laser that is diode-laser pumped. Unlike diode lasers, solid-state lasers are not typically guided-wave devices, and an active mode-locking

element must modulate an open beam. This has constrained such lasers to use bulk acousto-optical or electro-optical modulators, and, in turn, has limited the mode-locked pulse frequency to roughly 1 GHz. Recent research[Godil] has demonstrated mode locking of such a laser with a pulse rate of 20 GHz. The key element in this laser was a bulk $LiNbO_3$ phase modulator that was designed as a microwave cavity resonator. The particular laser that was demonstrated used Nd:BEL as the lasing medium and the pulse width for operation at 20 GHz was 3.9 ps. When pumped with 800 mW from a diode laser, the average power of the pulsed output was 30 mW. With improved coatings on the modulator, an output power 100 mW is expected. Also, by varying the design of the modulator, it is expected that mode locking could be accomplished over the range of 2 to 100 GHz. The properties of this new class of mode-locked solid-state laser appears to match well with the requirements of the HOE-ADC. However, the issue of stability remains untested.

5.2 Summary

To summarize the final results, an experimental simulation of a four-channel optical analog-to-digital converter (ADC) operating at 4 GS/s with 2-GHz bandwidth was conducted. The precision obtained in the bandpass sampling mode (near 10 GHz) was 3.8 bits. For baseband signals of up to 2 GHz, the measured precision was 4.6 bits. This performance exceeded the original program goals and constitutes the best known performance obtained with an optics-based ADC approach. The optical ADC technique developed offers potential performance of 10 GHz bandwidth, 20 gigasamples/sec (GS/s) sampling rate, and precision of 6 bits or more. A secondary result from the testing was the development of a data reduction methodology that revealed a previously unreported correlation between jitter and pulse-energy fluctuations. The calculated jitter was twice as small as that derived using a commonly used power spectral density analysis that assumes no correlation between these quantities. This new technique for determining jitter should be of value in future research in high-performance optical ADCs. Several publications have resulted from the work done under this contract (refs. 1-1,2,3).

6.0 REFERENCES

1-1. Bell, J. A., M. C. Hamilton, and D. A. Leep, "A/D Conversion of Microwave Signals Using a Hybrid Optical/Electronic Technique." *SPIE Proceedings* 1476, paper 1476-40 (1991). OE Aerospace Sensing Symposium, Orlando, Florida.

1-2. Bell, J. A., M. C. Hamilton, and D. A. Leep, "Optical Sampling and Demultiplexing Applied to A/D Conversion." *SPIE Proceedings* 1562 (1991): 276-81. SPIE Annual Symposium, San Diego, California.

1-3. Leep, D. A., and D. A. Holm, "Spectral Measurement of Timing JItter in Gain-Switched Semiconductor Lasers," *Applied Phyics. Letters* 60, no. 20: 2451.

1-4. Taylor, H. F., "An Electro-Optic Analog-to-Digital Converter." *Proc. IEEE* 63 (1975): 1524-1525.

1-5. Becker, R. A., C. E. Woodward, F. J. Leonberger, and R.C. Williamson, "Wide-Band Electro-Optic Guided-Wave Analog-to-Digital Converters." *Proc. IEE* 72, no. 7 (1984): 802-819.

2-1. Poulton, K., J. J. Corcoran and T. Hornak, "A 1-GHz 6-bit ADC System." *IEEE Solid-State Circuits* sc-22, no. 6 (1987): 962.

2-2. "Tektronix, Inc., Digitizing Signal Analyzer—DSA 602A." *Tektronix Catalog* (1991): 40-43.

2-3. Bowers, J. E. et al. "Actively Mode-Locked Semiconductor Lasers." *IEEE J. Quantum Electron.* 25, no. 6 (1989): 1426.

2-4. Taylor, A. J. et al."Timing Jitter in Mode-Locked and Gain-Switched InGaAsP Injection Lasers." *Applied Phyics Letters* 49, no. 12, (1986): 681.

2-5. Burns, D. et al. "Noise Characterization of a Mode-Locked InGaAsP Semiconductor Diode Laser." *IEEE J. Quantum Elec.* 26, no. 11 (1990): 1860.

2-6. Tucker, R. S., G. Eisenstein and S. K. Korotky, "Optical Time-Division Multiplexing For Very High Bit-Rate Transmission." *J. Lightwave Tech.* 6, no. 11, (1988): 1737.

3-1. Thaniyavarn, S., "A Synthesized Digital Switch Using a 1x2 Directional Coupler with Asymmetric Dß Phase Reversal Electrode." *IGWO*, paper TuC6-1 (1988): 252-55.

3-2. Thaniyavarn, S., "Modulation Diagrams of Coupled-Waveguide Interferometers and Directional Couplers." *SPIE* 835-35. OE/Fiber '87, San Diego, California, August 1987.